



Ballistic and Corrosion Analysis of New Military-Grade Magnesium Alloys AMX602 and ZAXE1711 for Armor Applications

**by Tyrone L. Jones, Joseph P. Labukas, Brian E. Placzankis,
and Katsuyoshi Kondoh**

ARL-TR-5931

February 2012

NOTICES

Disclaimers

The findings in this report are not to be construed as an official Department of the Army position unless so designated by other authorized documents.

Citation of manufacturer's or trade names does not constitute an official endorsement or approval of the use thereof.

Destroy this report when it is no longer needed. Do not return it to the originator.

Army Research Laboratory

Aberdeen Proving Ground, MD 21005-5066

ARL-TR-5931**February 2012**

Ballistic and Corrosion Analysis of New Military-Grade Magnesium Alloys AMX602 and ZAXE1711 for Armor Applications

Tyrone L. Jones, Joseph P. Labukas, and Brian E. Placzankis
Weapons and Materials Research Directorate, ARL

Katsuyoshi Kondoh
Osaka University

REPORT DOCUMENTATION PAGE				Form Approved OMB No. 0704-0188	
Public reporting burden for this collection of information is estimated to average 1 hour per response, including the time for reviewing instructions, searching existing data sources, gathering and maintaining the data needed, and completing and reviewing the collection information. Send comments regarding this burden estimate or any other aspect of this collection of information, including suggestions for reducing the burden, to Department of Defense, Washington Headquarters Services, Directorate for Information Operations and Reports (0704-0188), 1215 Jefferson Davis Highway, Suite 1204, Arlington, VA 22202-4302. Respondents should be aware that notwithstanding any other provision of law, no person shall be subject to any penalty for failing to comply with a collection of information if it does not display a currently valid OMB control number. PLEASE DO NOT RETURN YOUR FORM TO THE ABOVE ADDRESS.					
1. REPORT DATE (DD-MM-YYYY) February 2012		2. REPORT TYPE Final		3. DATES COVERED (From - To) 1 January 2009–30 November 2011	
4. TITLE AND SUBTITLE Ballistic and Corrosion Analysis of New Military-Grade Magnesium Alloys AMX602 and ZAXE1711 for Armor Applications				5a. CONTRACT NUMBER	
				5b. GRANT NUMBER	
				5c. PROGRAM ELEMENT NUMBER	
6. AUTHOR(S) Tyrone L. Jones, Joseph P. Labukas, Brian E. Placzankis, and Katsuyoshi Kondoh*				5d. PROJECT NUMBER	
				5e. TASK NUMBER	
				5f. WORK UNIT NUMBER	
7. PERFORMING ORGANIZATION NAME(S) AND ADDRESS(ES) U.S. Army Research Laboratory ATTN: RDRL-WMP-E Aberdeen Proving Ground, MD 21005-5066				8. PERFORMING ORGANIZATION REPORT NUMBER ARL-TR-5931	
9. SPONSORING/MONITORING AGENCY NAME(S) AND ADDRESS(ES)				10. SPONSOR/MONITOR'S ACRONYM(S)	
				11. SPONSOR/MONITOR'S REPORT NUMBER(S)	
12. DISTRIBUTION/AVAILABILITY STATEMENT Approved for public release; distribution is unlimited.					
13. SUPPLEMENTARY NOTES *Joining and Welding Research Institute (JWRI), Osaka University, 11-1 Mihogaoka, Ibaragi, Osaka, 567-0047, Japan					
14. ABSTRACT Since 2006, the U.S. Army has been evaluating magnesium (Mg) alloys for ballistic structural applications. While Mg alloys have been used in military structural applications since World War II, very little research has been done to improve their mediocre ballistic performance. The Army's need for ultra-lightweight armor systems has led to research and development of high-strength, high-ductility Mg alloys. The U.S. Army Research Laboratory (ARL) and the Joining and Welding Research Institute (JWRI) of Osaka University collaborated to develop the next generation of high-strength, high-ductility Mg alloys using a novel Spinning Water Atomization Process for rapid solidification. New alloys AMX602 and ZAXE1711 in extruded bar form are characterized for microstructure, mechanical, corrosion resistance, and ballistic response. Corrosion evaluations included neutral salt fog, GM 9540P, and cyclic polarization comparisons. Increases in ballistic performance and favorable corrosion resistance were evident when compared to the baseline armor alloy AZ31B.					
15. SUBJECT TERMS magnesium, armor, corrosion, ballistics, AZ31B, AMX602, ZAXE1711, salt fog, potentiodynamic polarization, GM9540P					
16. SECURITY CLASSIFICATION OF:			17. LIMITATION OF ABSTRACT UU	18. NUMBER OF PAGES 60	19a. NAME OF RESPONSIBLE PERSON Tyrone L. Jones
a. REPORT Unclassified	b. ABSTRACT Unclassified	c. THIS PAGE Unclassified			19b. TELEPHONE NUMBER (Include area code) 410-278-6223

Contents

List of Figures	v
List of Tables	vii
Acknowledgments	viii
1. Introduction	1
2. Experimental Procedure	2
2.1 Alloy Synthesis.....	2
2.2 Experimental Evaluation of Raw Materials	3
2.3 Powder Consolidation	3
2.4 Mechanical Properties	4
2.5 Ballistic Evaluation	5
2.6 Accelerated Corrosion Exposure and Mass Loss Measurements.....	6
2.7 Cyclic Polarization Evaluations	8
3. Results	8
3.1 Ballistics	8
3.2 Accelerated Corrosion Exposure and Mass Loss	10
3.2.1 AZ31B	20
3.2.2 AMX602.....	20
3.2.3 ZAXE1711	20
3.3 Cyclic Polarization Results	21
4. Discussion	23
5. Conclusions	25
6. Future Work	25
7. References	26
Appendix A. AMX602 Ballistic Data and Pictures	29

Appendix B. ZAXE1711 Ballistic Data and Pictures	37
Distribution List	44

List of Figures

Figure 1. AZ31B grain size vs. impact energy absorption.	2
Figure 2. (a) Schematic illustration of SWAP equipment to produce rapidly solidified Mg alloy powders; (b) morphology of coarse magnesium alloy powder prepared by SWAP.....	3
Figure 3. The 0.30-cal. FSP schematic diagram.	5
Figure 4. Corrosion rack configuration used for neutral salt fog and GM 9540P exposures.	6
Figure 5. Post-ballistic pictures of front surface of (a) AMX602-1, (b) AMX602-2, and (c) AMX602-3 against 0.30-cal. FSP.	9
Figure 6. Post-ballistic pictures of back surface of (a) AMX602-1, (b) AMX602-2, and (c) AMX602-3 against 0.30-cal. FSP.	9
Figure 7. Post-ballistic pictures of target fronts (top) and backs (lower) of (a) ZAXE1711-B, (b) ZAXE-1711C, and (c) ZAXE-1711-D against 0.30-cal. FSP.....	9
Figure 8. Neutral salt fog corrosion of AZ31B-H24 at 18, 72, and 168 h.	10
Figure 9. GM 9540P cyclic corrosion of AZ31B-H24 at 1, 5, and 10 cycles.....	10
Figure 10. Neutral salt fog corrosion of AMX602-1 at 18, 72, and 168 h.	11
Figure 11. GM 9540P cyclic corrosion of AMX602-1 at 1, 5, and 10 cycles.	11
Figure 12. Neutral salt fog corrosion of AMX602-2 at 18, 72, and 168 h.	11
Figure 13. GM 9540P cyclic corrosion of AMX602-2 at 1, 5, and 10 cycles.	12
Figure 14. Neutral salt fog corrosion of AMX602-3 at 18, 72, and 168 h.	12
Figure 15. GM 9540P cyclic corrosion of AMX602-3 at 1, 5, and 10 cycles.	12
Figure 16. Neutral salt fog corrosion of ZAXE1711-B at 18, 72, and 168 h.	13
Figure 17. GM 9540P cyclic corrosion of ZAXE1711-B at 1, 5, and 10 cycles.	13
Figure 18. Neutral salt fog corrosion of ZAXE1711-C at 18, 72, and 168 h.	13
Figure 19. GM 9540P cyclic corrosion of ZAXE1711-C at 1, 5, and 10 cycles.	14
Figure 20. Neutral salt fog corrosion of ZAXE1711-D at 18, 72, and 168 h.	14
Figure 21. GM 9540P cyclic corrosion of ZAXE1711-C at 1, 5, and 10 cycles.	14
Figure 22. Corrosion rates in mpy based upon mass loss measurements after neutral salt fog (red) and GM 9540P cyclic corrosion exposures (blue).	15
Figure 23. Front surface of 168 h neutral salt fog specimens after cleaning to reveal extent of substrate loss.	16
Figure 24. Rear surfaces of 168 h neutral salt fog specimens after cleaning to reveal extent of substrate loss.	17
Figure 25. Front surfaces of 10 cycle GM 9540P cyclic corrosion specimens after cleaning to reveal extent of substrate loss.	18

Figure 26. Rear surfaces of 10 cycle GM 9540P cyclic corrosion specimens after cleaning to reveal extent of substrate loss.	19
Figure 27. Potentiodynamic polarization of AMX602-3, ZAXE1711-D, and AZ31B alloys.....	21
Figure 28. Potentiodynamic polarization of AMX602 and AZ31B alloys.....	22
Figure 29. Potentiodynamic polarization of ZAXE1711 and AZ31B alloys.....	22
Figure 30. Corrosion rate as function of composition for Mg alloy AZ91E with a quaternary alloying addition. Testing in 0.1M NaCl pH 6.	24

List of Tables

Table 1. Mechanical properties/goals of Mg alloys.....	1
Table 2. Chemical compositions of AMX602 and ZAXE1711 magnesium alloy powders.....	3
Table 3. Temper designations and temperatures for AMX602 and ZAXE1711.	4
Table 4. Mechanical properties for Mg alloy AMX602.	4
Table 5. Mechanical properties for Mg alloy ZAXE1711.....	4
Table 6. Projectile weight and hardness requirements.....	5
Table 7. Thickness and Brinell hardness of each MG alloy test bar.....	6
Table 8. GM 9540P cyclic corrosion test details.	7
Table 9. Mg alloy V_{50} ballistic velocities against 0.30-cal. FSP.	9

Acknowledgments

The authors wish to recognize the laboratory assistance of Chris Miller and Tom Considine, who assisted with the chambers and the mass loss determinations.

1. Introduction

The U.S. Army Research Laboratory's (ARL's) ballistic assessment of magnesium (Mg) alloys over the last 5 years has led to an increased understanding of the material's failure mechanisms and relationship between Mg alloy strength and ductility requirements for lightweight armor applications (1). While Mg alloys have been used for military structural applications since World War II, very little research has been done to improve their mediocre ballistic performance (2). The highest strength commercial Mg alloy available in plate form, AZ31B, has proven to be a very good substitute armor material for AA5083 against armor-piercing projectiles on an equal weight basis (3). For specific areal density ranges, AZ31B is an adequate substitute armor material against fragment-simulating projectiles (FSPs) (4). The ballistic data generated by ARL was used to develop the first set of Mg alloy acceptance standards, MIL-DTL-32333 (MR), titled *Armor Plate, Magnesium Alloy, AZ31B, Applique* (5). Ultimate tensile strength, tensile yield strength, ductility, and grain size are all key performance parameters in determining the ballistic performance of these metals. The bulk material properties of AZ31B are shown in table 1.

Table 1. Mechanical properties/goals of Mg alloys.

Alloy	Ultimate Tensile Strength (MPa)	Tensile Yield Strength (MPa)	Elongation to Failure (%)
AZ31B	245	150	7
Proposed Mg alloy	400	350	20

In 2009, ARL collaborated with the Joining and Welding Research Institute (JWRI) of Osaka University under contract through International Technology Center-Pacific to develop and evaluate high-strength, high-ductility Mg alloy plate for structural applications. An initial evaluation of conventionally rolled AZ31B plate vs. powder-formed AZ31B plate showed that conventional processing, tempering, and grain refinement will not significantly improve the ballistic performance of this particular Mg armor alloy (6). Prior examination also showed that there was a range of optimal powder grain sizes to absorb the impact energy (figure 1) (7).

Although AZ31B compares favorably with AA5083 for armor plates (4), improved Mg alloys would be required in order to better compete with the improved aluminum (Al) armor alloy solutions. New fundamental Mg alloying is needed to increase the impact energy and thus the performance of Mg alloy plates. Based on preliminary material and ballistic analysis, the ARL/JWRI program set goals to develop Mg alloys with the mechanical properties shown in table 1.

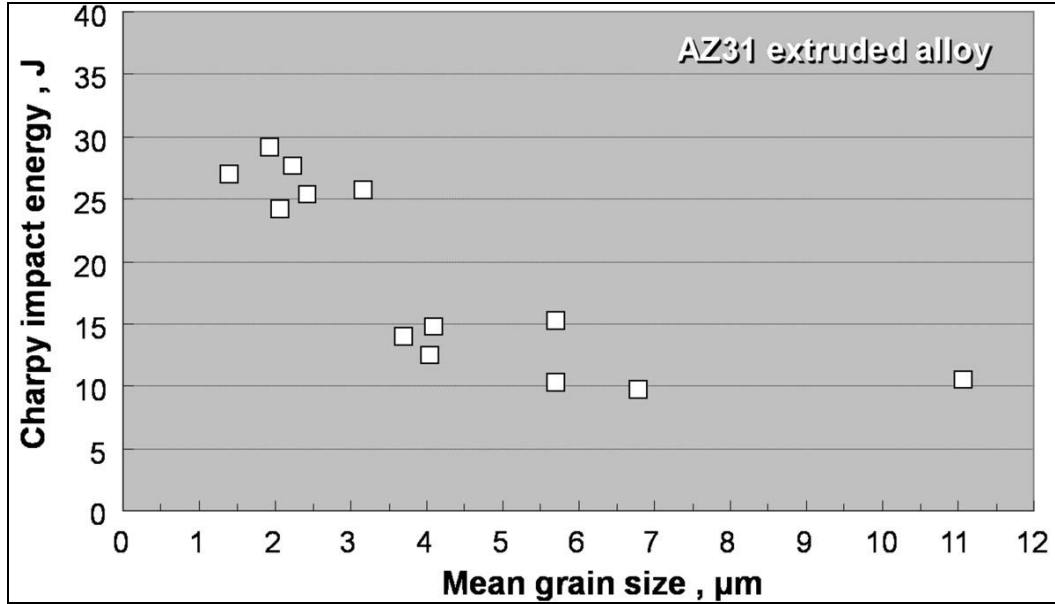


Figure 1. AZ31B grain size vs. impact energy absorption.

Clearly, there were two potential paths toward achieving these set goals:

1. Create new chemical compositions to develop high-strength, high-ductility Mg alloys.
2. Improve grain refinement through novel processing techniques to produce high-strength, high-ductility Mg alloys.

As a result, ARL and JWRI collaboratively developed two new experimental Mg alloys, AMX602 and ZAXE1711, using an advanced metallurgical powder process. The initial material development and ballistic evaluation of Mg alloys AMX602 and ZAXE1711 are discussed in the next sections.

2. Experimental Procedure

2.1 Alloy Synthesis

AMX602 (Mg-6Al-0.5Mn-2Ca/mass%) and ZAXE1711 (Mg-1Zn-7Al-1Ca-1La/mass%) Mg alloy powders produced by the Spinning Water Atomization Process (SWAP) were used as raw input materials (8, 9). The coarse Mg alloy powders were 1–5 mm long. It was previously verified that the coarse Mg powders of these lengths were noncombustible. The α -Mg grain size of the raw powders was $<0.5 \mu\text{m}$. The powder compaction and hot extrusion were applied to these raw powders to fabricate the extruded bars. The bars had a cross section of $24.5 \times 40 \times 1000 \text{ mm}$. Tensile test specimens machined from these bars were evaluated at room temperature. The microstructural analyses of the materials are available in previous manuscripts (10, 11).

2.2 Experimental Evaluation of Raw Materials

In SWAP powder preparation, schematically illustrated in figure 2a, noncombustive AMX602 Mg alloy ingots were melted at 1053 K in a ceramic crucible purged with argon. The molten metals were directly streamed inside the spinning water chamber from the crucible nozzle. Table 2 shows chemical compositions of AMX602 alloy powders prepared by SWAP. The calcium (Ca) is necessary because it promotes the noncombustive properties of the Mg alloys. The impurity content of iron (Fe) and copper (Cu) is controlled to <0.005% because the elements are corrosive in Mg alloys. As shown in figure 2b, a length of the coarse, irregularly shaped AMX602 powders prepared by SWAP is ~1–4 mm. A cast ingot with the same composition was also prepared as a reference input material.

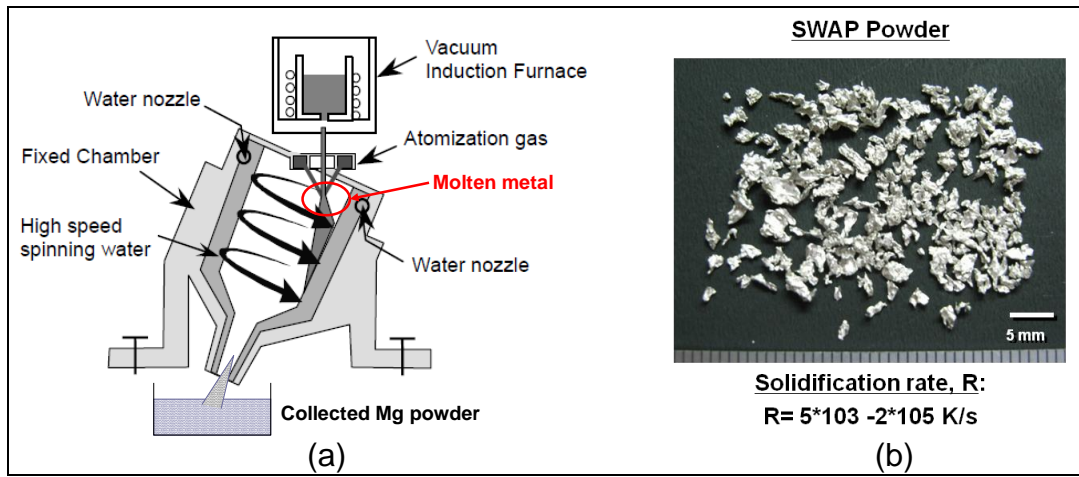


Figure 2. (a) Schematic illustration of SWAP equipment to produce rapidly solidified Mg alloy powders and (b) morphology of coarse Mg alloy powder prepared by SWAP.

Table 2. Chemical compositions of AMX602 and ZAXE1711 Mg alloy powders.

Alloy	Al	Mn	Zn	Ca	La	Si	Cu	Ni	Fe	Others
AZ31B	2.5–3.5	0.2–1.0	0.6–1.4	0.04 max	—	0.1 max	0.05 max	0.005 max	0.005 max	0.30 max
AMX602	6.0	0.5	—	2.0	—	—	—	—	—	—
ZAXE1711	7.0	—	1.0	1.0	1.0	—	—	—	—	—

2.3 Powder Consolidation

The powder was consolidated at room temperature using a 2000-kN hydraulic press to fabricate the green compact. The green compact had a relative density of 85% and was 42 mm in diameter. The columnar compact and cast ingot were heated to between 573 and 673 K for 180 s in an argon atmosphere, then immediately consolidated into full density material by hot extrusion. An extrusion ratio of 37 and an extrusion speed of 1 m/s were used in this study.

2.4 Mechanical Properties

Mg alloy AMX602 and ZAXE1711 bars of three different tempers were produced for ballistic evaluation. The temper designations (i.e., AMX602 temper) for each Mg alloy extrusion temperature are listed in table 3. The mechanical properties of the Mg alloy AMX602 and ZAXE1711 samples are shown in tables 4 and 5.

Table 3. Temper designations and temperatures for AMX602 and ZAXE1711.

Designation and Tempering Temperature (°C)	
AMX602	ZAXE1711
1: 350	B: 350
2: 300	C: 250
3: 250	D: 200

Table 4. Mechanical properties for Mg alloy AMX602.

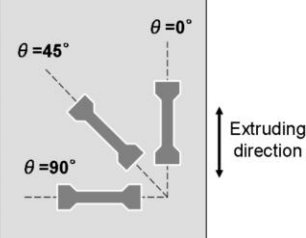
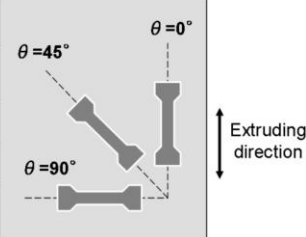
	0° - center			0° - 1/4 width			45°			90°			
	σ	σ_y	EI	σ	σ_y	EI	σ	σ_y	EI	σ	σ_y	EI	
	MPa	MPa	%	MPa	MPa	%	MPa	MPa	%	MPa	MPa	%	
Rod 1	355	301	21.0	359	306	19.2	319	234	18	330	244	16.4	
Rod 2	357	314	20.8	363	302	18.0	323	236	22.4	307	237	8.5	
Rod 3	358	311	17.8	360	312	19.1	324	261	15.1	304	244	7.6	

Table 5. Mechanical properties for Mg alloy ZAXE1711.

	0° - center			0° - 1/4 width			45°			90°			
	σ	σ_y	EI	σ	σ_y	EI	σ	σ_y	EI	σ	σ_y	EI	
	MPa	MPa	%	MPa	MPa	%	MPa	MPa	%	MPa	MPa	%	
Rod B	377	268	17.4	380	276	17.4	356	245	15.8	363	248	13.0	
Rod C	380	269	18.2	384	280	18.4	361	245	18.7	369	246	18.2	
Rod D	388	274	18.7	391	286	18.3	362	238	22.5	374	236	19.4	

The differences between the mechanical properties in different extruding directions, at the selected tempers, are very small for Mg alloys AMX602 and ZAXE1711. Therefore, the extrusion temperature was not considered a significant factor for strength when fabricating the scale-up specimens.

All V_{50} ballistic limits (velocity at which the projectile is expected to perforate the armor 50% of the time) were calculated following MIL-STD-662F (12). Based on the aforementioned MIL-DTL-32333 (5) baseline thickness requirements, the Mg alloy bars were evaluated using the 0.30-cal. FSP (13). The test projectile schematic diagram, weights, and hardness specifications are shown in table 6 and figure 3. Prior to ballistic evaluations, the hardness of each target Mg alloy test bar was measured using the 500-kg Brinell scale. The targets were held horizontally in a test fixture by C-clamps on the ends of the bars. The thickness and nominal hardness of each Mg alloy test bar is shown in table 7. In the instances where multiple bars of an alloy were tested, i.e., AMX602-1, a “/” is used to separate thickness and hardness.

FSP Type	Weight (g)	Rockwell C Hardness
0.30 cal.	44.0 ± 0.5	30 ± 2



Table 7. Thickness and Brinell hardness of each Mg alloy test bar.

Metal Alloys	Thickness (mm)	Hardness ^a (HBN)
AZ31B	25.4	61
AMX602-1	25.190/25.235	80/80
AMX602-2	25.171/25.210/25.197	80/80/83
AMX602-3	25.171/25.178	80/80
ZAXE1711-B	25.248	80
ZAXE1711-C	25.229/25.241	77/83
ZAXE1711-D	25.210/25.279	80/80

^aMeasured on a 500-kg scale.

2.6 Accelerated Corrosion Exposure and Mass Loss Measurements

In order to assess the inherent corrosion resistance capabilities of the bare, unprotected AMX602 and the ZAXE1711 alloys, specimens were sectioned to 1.75- × 1.5- × 0.25-in nominal dimensions from the target bars using a water-cooled nonmetallic abrasive blade saw. For increased precision in mass loss measurements to determine corrosion rates, additional milling was used to ensure the 0.25-in thickness. All specimens were then surface finished with 600 grit using metallographic grinding techniques. Following grinding, all specimens were cleaned and rinsed using acetone. In order to normalize weight loss data collected among the specimens, the surface areas were measured in addition to the initial masses. Finally, following the measurements for dimensions and mass, the specimens were organized in racks as shown in figure 4 and then placed into their respective chambers.



Figure 4. Corrosion rack configuration used for neutral salt fog and GM 9540P exposures.

A standard wet-bottom style test chamber was used for neutral salt fog testing, and a cyclic corrosion chamber was used for cyclic testing. The neutral salt fog operating parameters were in accordance with ASTM B 117 (14) at 95 °F with saturated humidity and an atomized fog of 5% sodium chloride (NaCl) solution. The observation and scanning intervals for the specimens in neutral salt fog were set to 18, 72, and 168 h. The GM 9540P (15) cyclic accelerated corrosion test consisted of 18 separate stages that included saltwater spray using 0.9% NaCl, 0.1% CaCl₂, 0.25% NaHCO₃ test solution, high humidity, drying, ambient, and heated drying. The environmental conditions and duration of each stage for one complete cycle are provided in table 8.

Table 8. GM 9540P cyclic corrosion test details (15).

Interval	Description	Time (min)	Temperature (± 3 °C)
1	Ramp to salt mist	15	25
2	Salt mist cycle	1	25
3	Dry cycle	15	30
4	Ramp to salt mist	70	25
5	Salt mist cycle	1	25
6	Dry cycle	15	30
7	Ramp to salt mist	70	25
8	Salt mist cycle	1	25
9	Dry cycle	15	30
10	Ramp to salt mist	70	25
11	Salt mist cycle	1	25
12	Dry cycle	15	30
13	Ramp to humidity	15	49
14	Humidity cycle	480	49
15	Ram to dry	15	60
16	Dry cycle	480	60
17	Ram to ambient	15	25
18	Ambient cycle	480	25

Although the GM 9540P procedure was developed for steel substrates, previous studies (16) have shown that the cyclic nature of the exposure and the electrolyte used can also have a significant corrosion impact on Mg alloys. The observation and scanning intervals for the GM 9540P specimens were 1, 5, and 10 cycles.

In order to visually assess and characterize the corrosion, all specimens were scanned at 800 dots per inch (dpi) optical resolution at their respective intervals using color flatbed scanning techniques. In order to better reveal the corrosion damage to the substrate surface, the specimens were vigorously rinsed under a stream of deionized water to remove loose corrosion products. Following the rinse, the specimens were then allowed to dry prior to scanning. After the final scan at the conclusion of exposures in neutral salt fog and GM 9540P, the specimens were all cleaned in accordance with ASTM G 97 (17) to remove all remaining corrosion products prior to final weighing to determine the mass loss followed by a final postcleaning scan of the front and rear sides of the specimens. After the final weights were obtained, the corrosion rate in mils per year (mpy) was then calculated using the following formula:

$$\text{mpy} = \frac{K \times (m_i - m_f)}{(A \times T \times d)}, \quad (1)$$

where

K = constant (546,000 for mpy),

m_i = initial mass (g),

m_f = final mass (g),

A = area (in^2),

T = time (h), and

D = density (g/cm^3).

For GM 9540P cyclic corrosion where duration is measured in cycles, each cycle was normalized to 24 h. Therefore, the final exposure time in hours for the GM 9540P specimens was 240 h.

2.7 Cyclic Polarization Evaluations

The Mg alloy specimen surfaces were polished with wet 600-grit sandpaper, rinsed with deionized water, and dried with a stream of nitrogen prior to electrochemical measurements. A Princeton Applied Research flat cell that comprised an Mg alloy as the working electrode (1 cm^2), platinum-coated wire mesh as the counter electrode, and a saturated calomel electrode as the reference electrode was used for potentiodynamic polarization in 3.5% NaCl (aq) solution. Nitrogen was bubbled through the solution in the cell for 20 min prior to polarization of the sample. Gamry Framework software was used to measure the open circuit potential (OCP) for 10 s and subsequently polarize the working electrode from -0.5 to 0.5 V of the OCP at 10 mV/s .

3. Results

3.1 Ballistics

As evident in figures 5–7, the Mg AMX602 and Mg ZAXE1711 bars showed reasonable ductility under ballistic impact. For the instances when the projectile perforated the Mg AMX602 or Mg ZAXE1711 bars and created an exit hole, the spall was typically localized within a 32-mm diameter. Although the edge of the spall after ballistic impact reached the edge of the AMX602 and ZAXE1711 bars, the V_{50} data significantly exceeded Mg alloy AZ31B V_{50} data at the same areal weight while maintaining its structural integrity. The V_{50} data are shown in table 9. Mg alloy AMX602 showed up to a 33% increase in the V_{50} ballistic limit compared to Mg armor alloy AZ31B (attained from MIL-DTL-32333 [5]), while Mg alloy ZAXE1711 showed up to a 37% increase in the V_{50} ballistic limit compared to Mg armor alloy AZ31B.

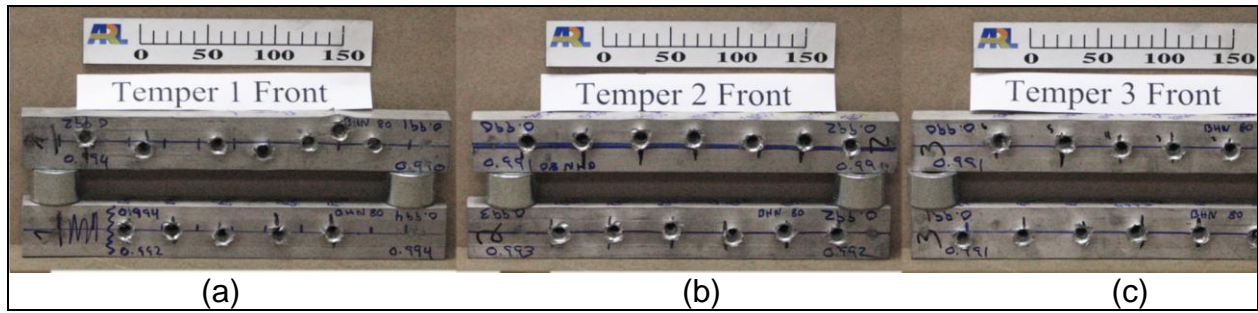


Figure 5. Postballistic pictures of front surface of (a) AMX602-1, (b) AMX602-2, and (c) AMX602-3 against 0.30-cal. FSP.

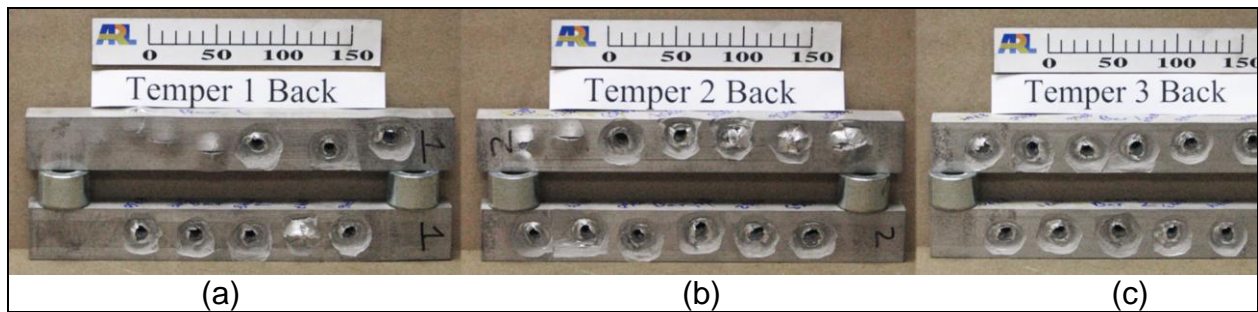


Figure 6. Postballistic pictures of back surface of (a) AMX602-1, (b) AMX602-2, and (c) AMX602-3 against 0.30-cal. FSP.

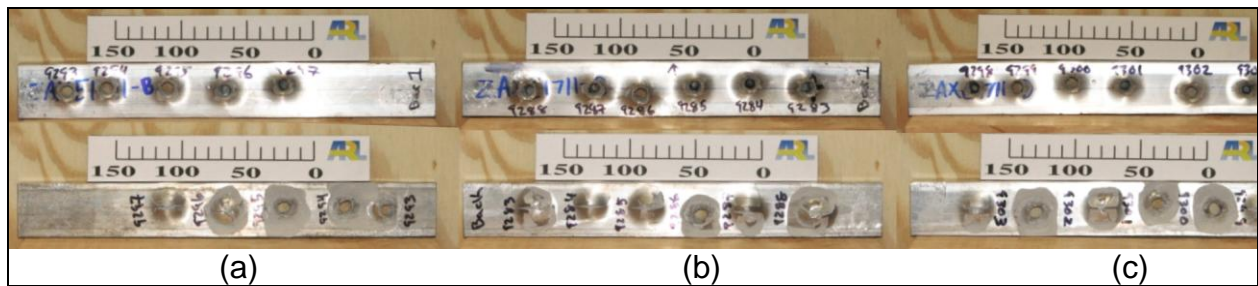


Figure 7. Postballistic pictures of target fronts (top) and backs (lower) of (a) ZAXE1711-B, (b) ZAXE-1711C, and (c) ZAXE-1711-D against 0.30-cal. FSP.

Table 9. Mg alloy V_{50} ballistic velocities against 0.30-cal. FSP.

Mg Alloys	Ballistic Limit (m/s)	Ballistic Limit (ft/s)
AZ31B	833	2733
AMX602-1	1061	3480
AMX602-2	1092	3570
AMX602-3	1105	3624
ZAXE1711-B	1111	3646
ZAXE1711-C	1117	3663
ZAXE1711-D	1140	3737

3.2 Accelerated Corrosion Exposure and Mass Loss

Figures 8–21 chronicle the progression of corrosion of AZ31B-H24, and the various tempers of the AMX602 and ZAXE1711 alloys in neutral salt fog and GM 9540P cyclic corrosion.

Figure 22 includes plots for corrosion rates determined through mass loss in neutral salt fog and GM 9540P. Figures 23–26 present the front and rear sides of final ASTM G 97 (17)-cleaned specimens to reveal the variety and extent of the corrosion damage from 168 h of neutral salt fog and 10 cycles of GM 9540P.

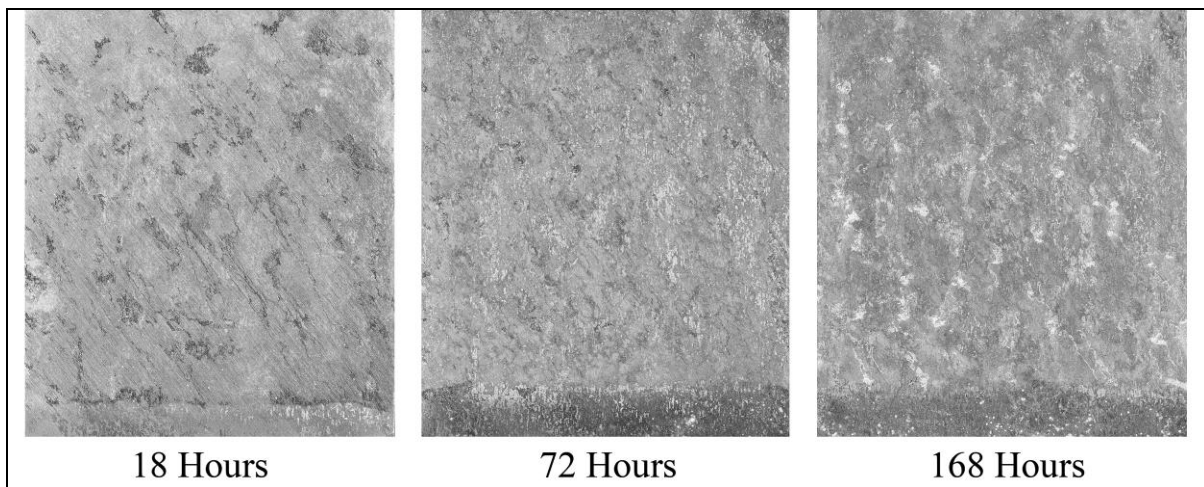


Figure 8. Neutral salt fog corrosion of AZ31B-H24 at 18, 72, and 168 h.

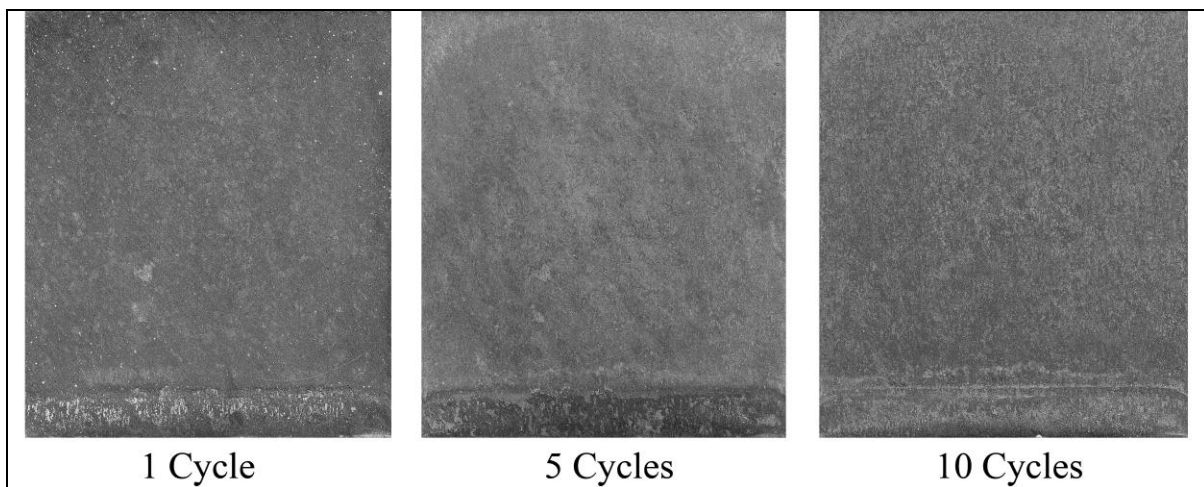


Figure 9. GM 9540P cyclic corrosion of AZ31B-H24 at 1, 5, and 10 cycles.

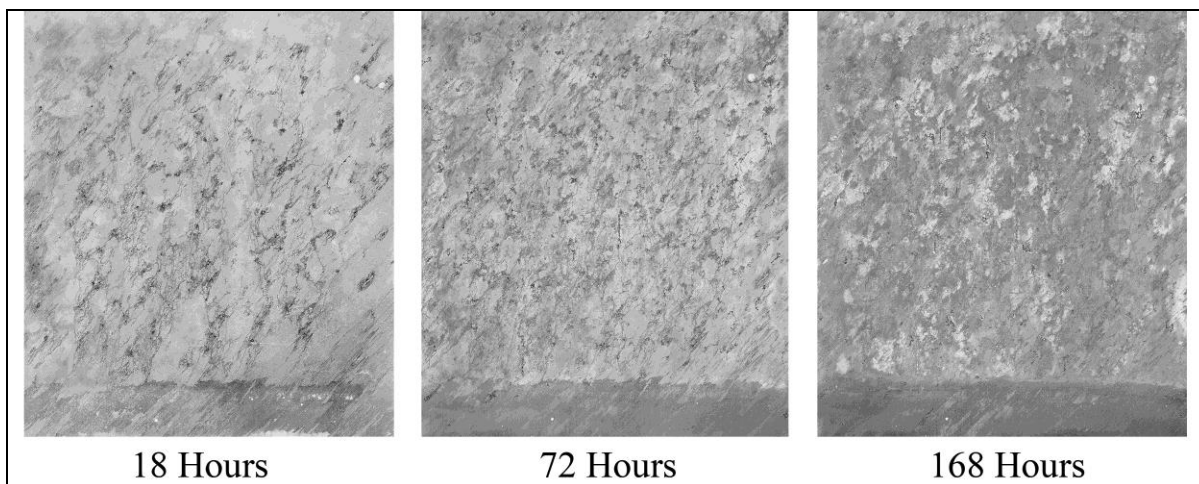


Figure 10. Neutral salt fog corrosion of AMX602-1 at 18, 72, and 168 h.

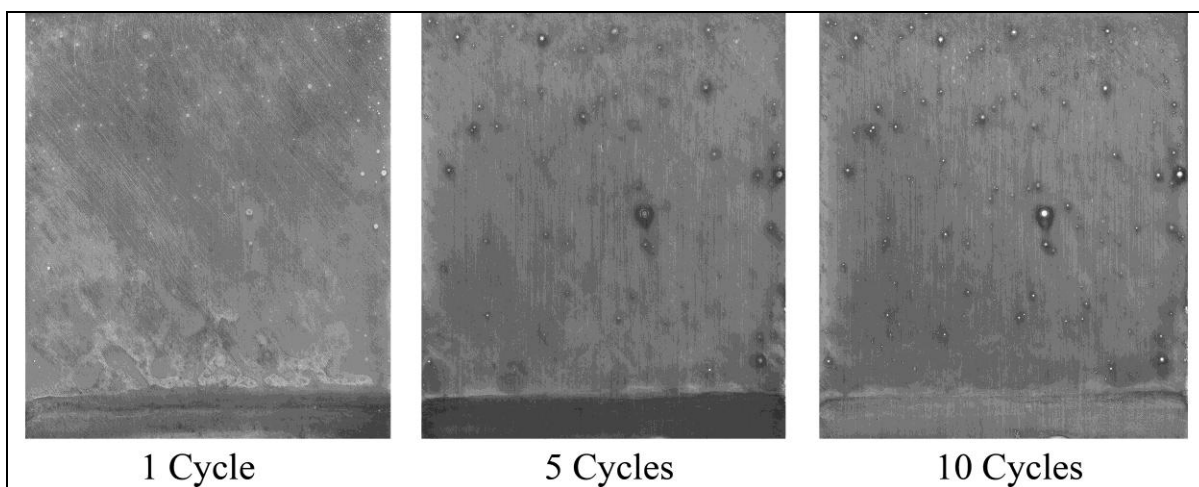


Figure 11. GM 9540P cyclic corrosion of AMX602-1 at 1, 5, and 10 cycles.

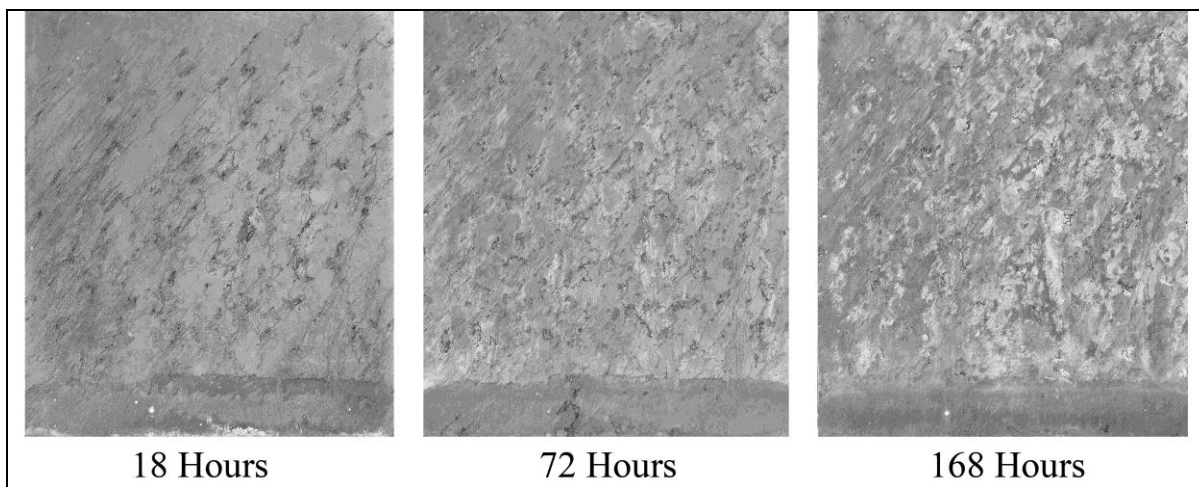


Figure 12. Neutral salt fog corrosion of AMX602-2 at 18, 72, and 168 h.

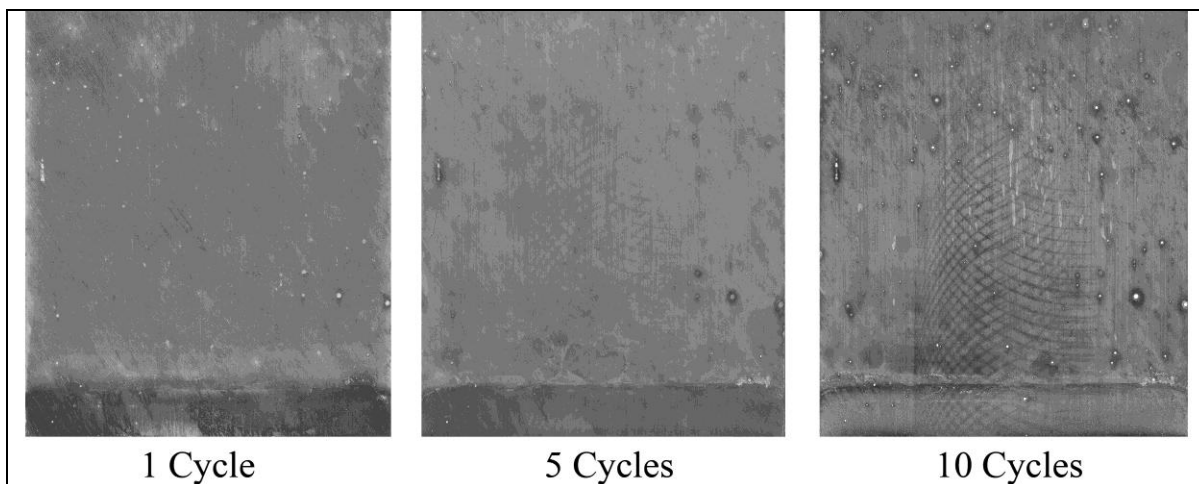


Figure 13. GM 9540P cyclic corrosion of AMX602-2 at 1, 5, and 10 cycles.

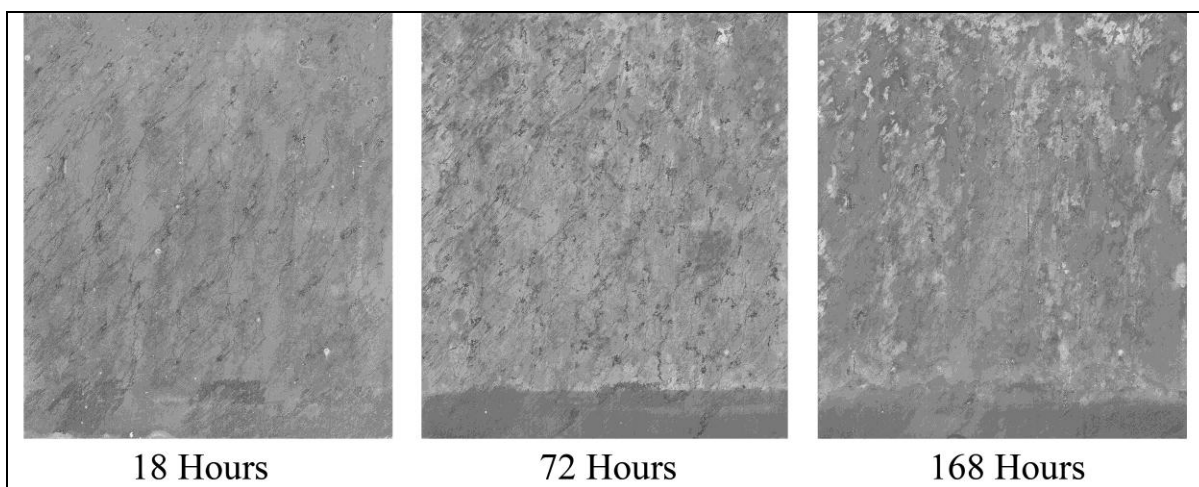


Figure 14. Neutral salt fog corrosion of AMX602-3 at 18, 72, and 168 h.

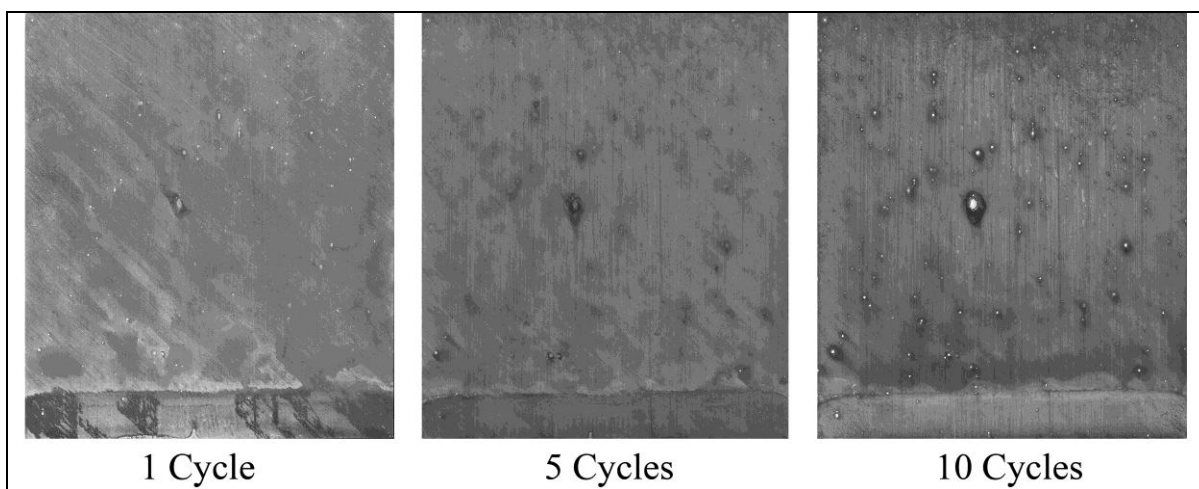


Figure 15. GM 9540P cyclic corrosion of AMX602-3 at 1, 5, and 10 cycles.

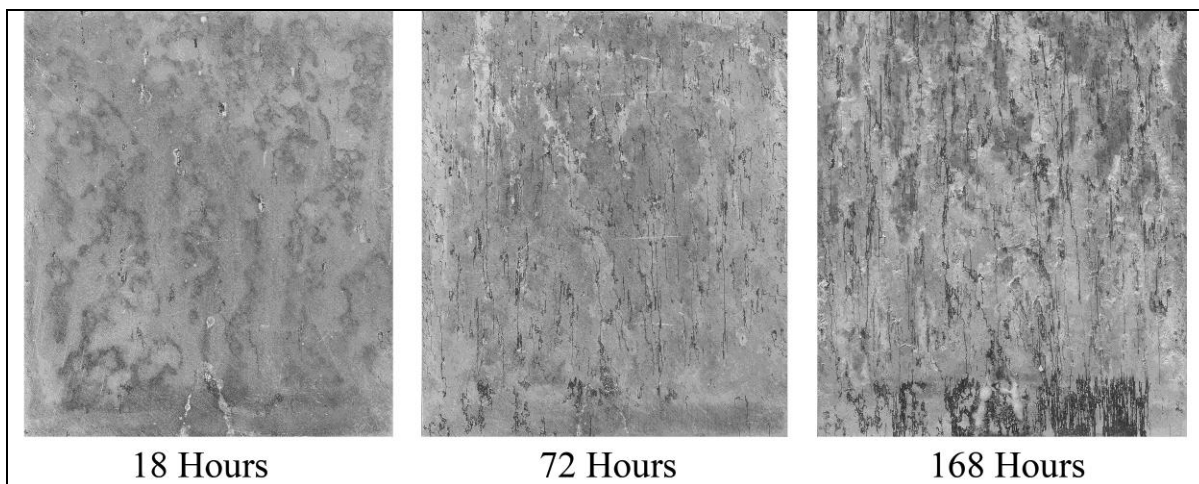


Figure 16. Neutral salt fog corrosion of ZAXE1711-B at 18, 72, and 168 h.

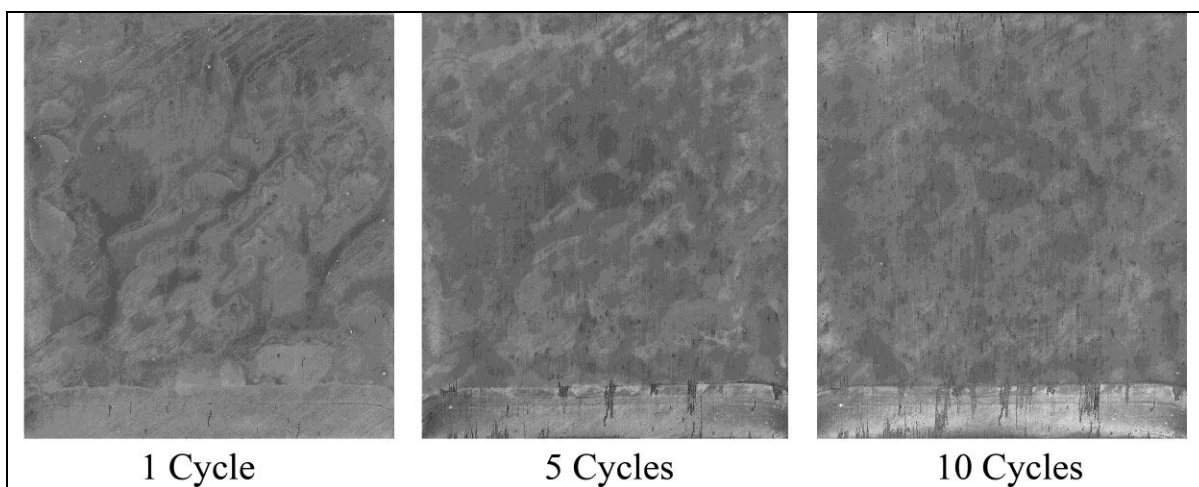


Figure 17. GM 9540P cyclic corrosion of ZAXE1711-B at 1, 5, and 10 cycles.

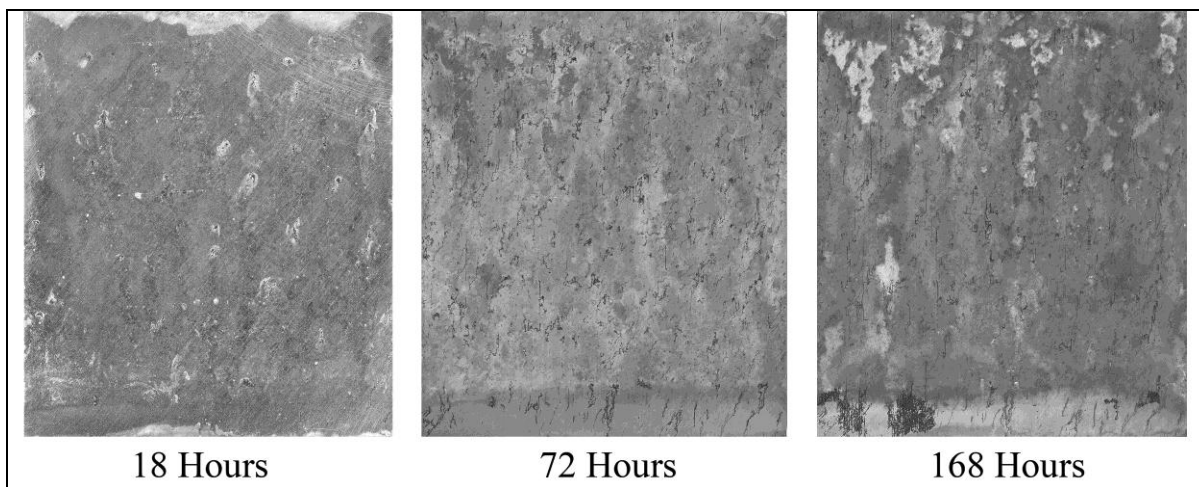


Figure 18. Neutral salt fog corrosion of ZAXE1711-C at 18, 72, and 168 h.

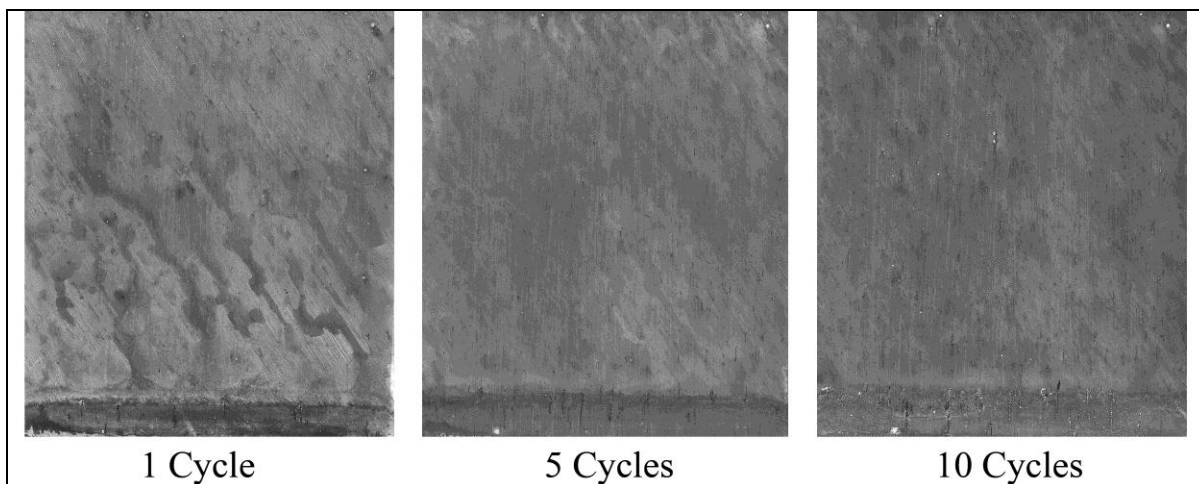


Figure 19. GM 9540P cyclic corrosion of ZAXE1711-C at 1, 5, and 10 cycles.

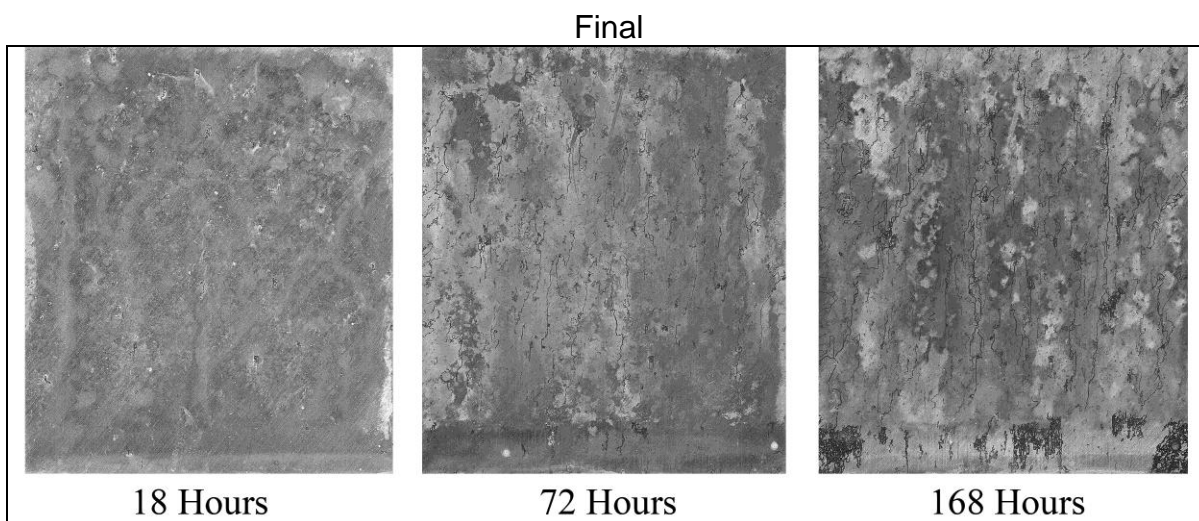


Figure 20. Neutral salt fog corrosion of ZAXE1711-D at 18, 72, and 168 h.

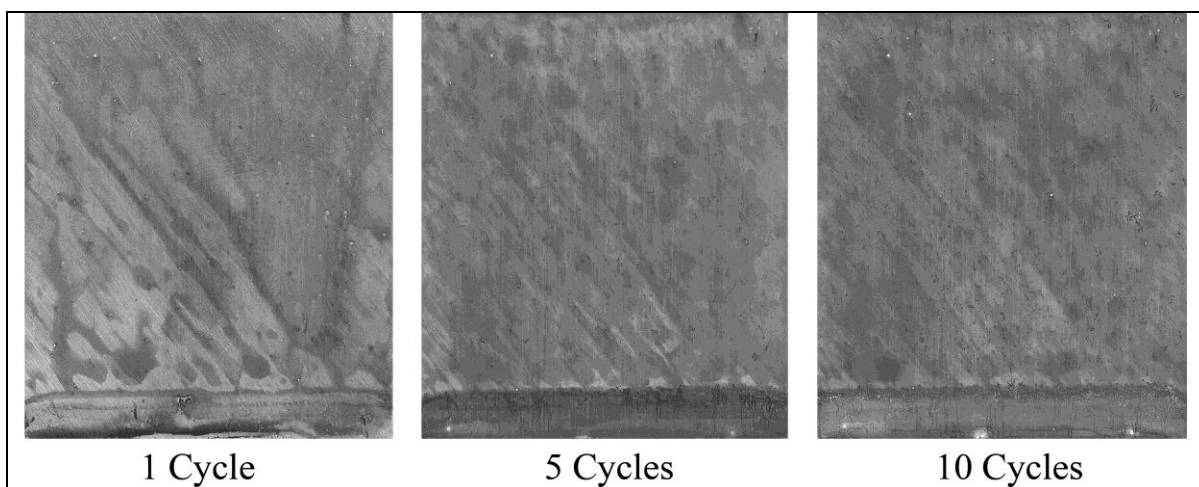


Figure 21. GM 9540P cyclic corrosion of ZAXE1711-C at 1, 5, and 10 cycles.

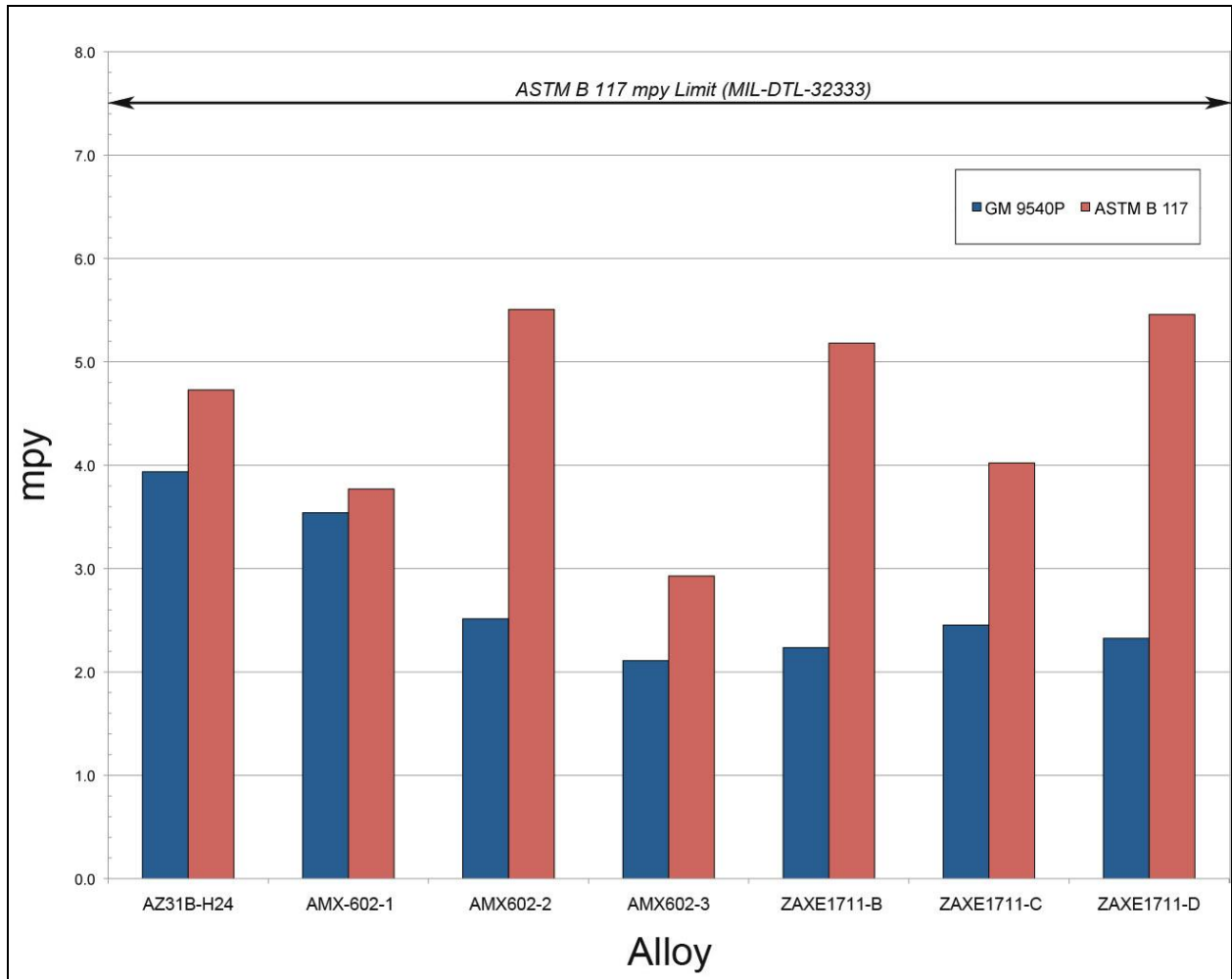


Figure 22. Corrosion rates in mils per year based upon mass loss measurements after neutral salt fog (red) and GM 9540P cyclic corrosion exposures (blue).

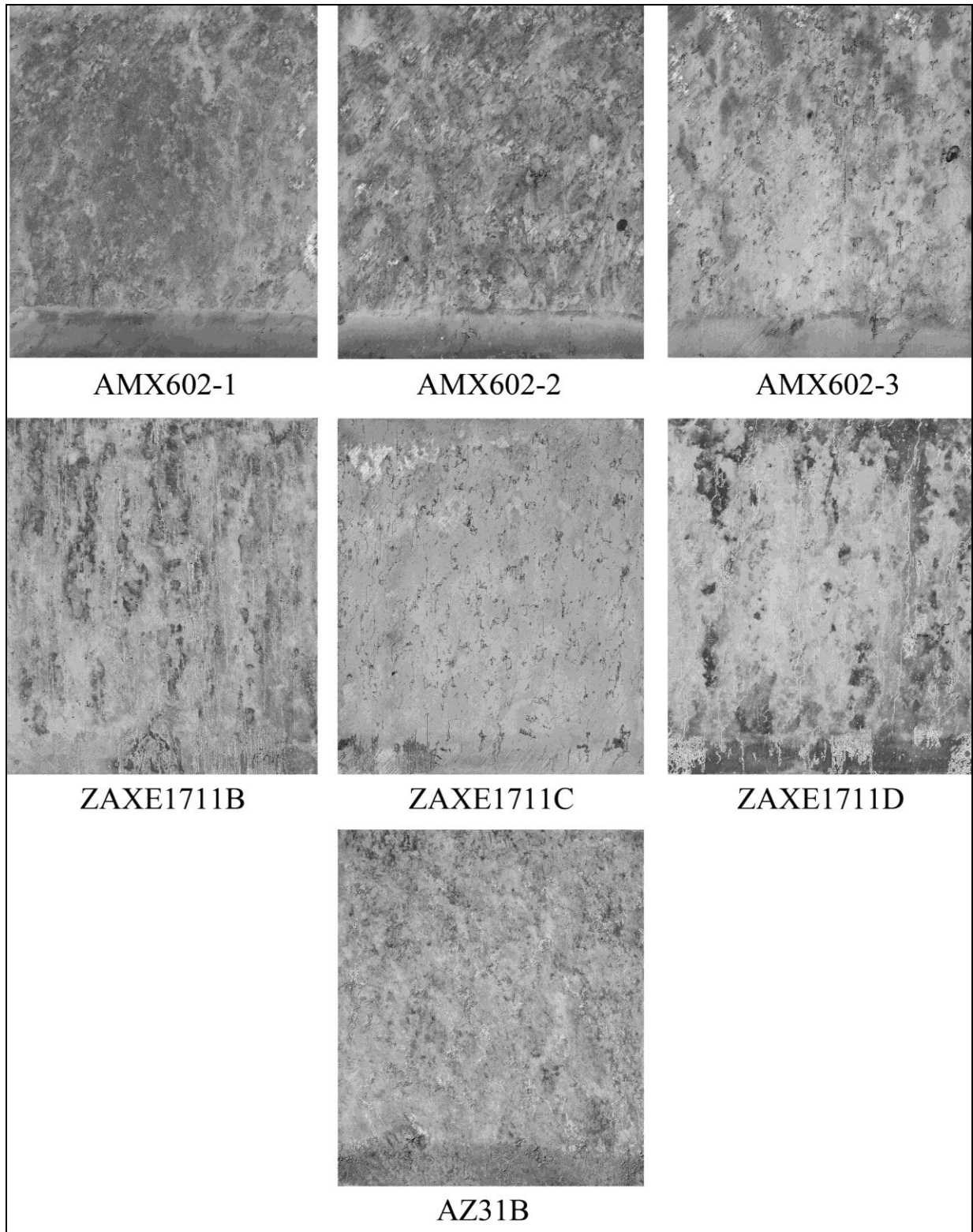


Figure 23. Front surface of 168-h neutral salt fog specimens after cleaning to reveal extent of substrate loss.

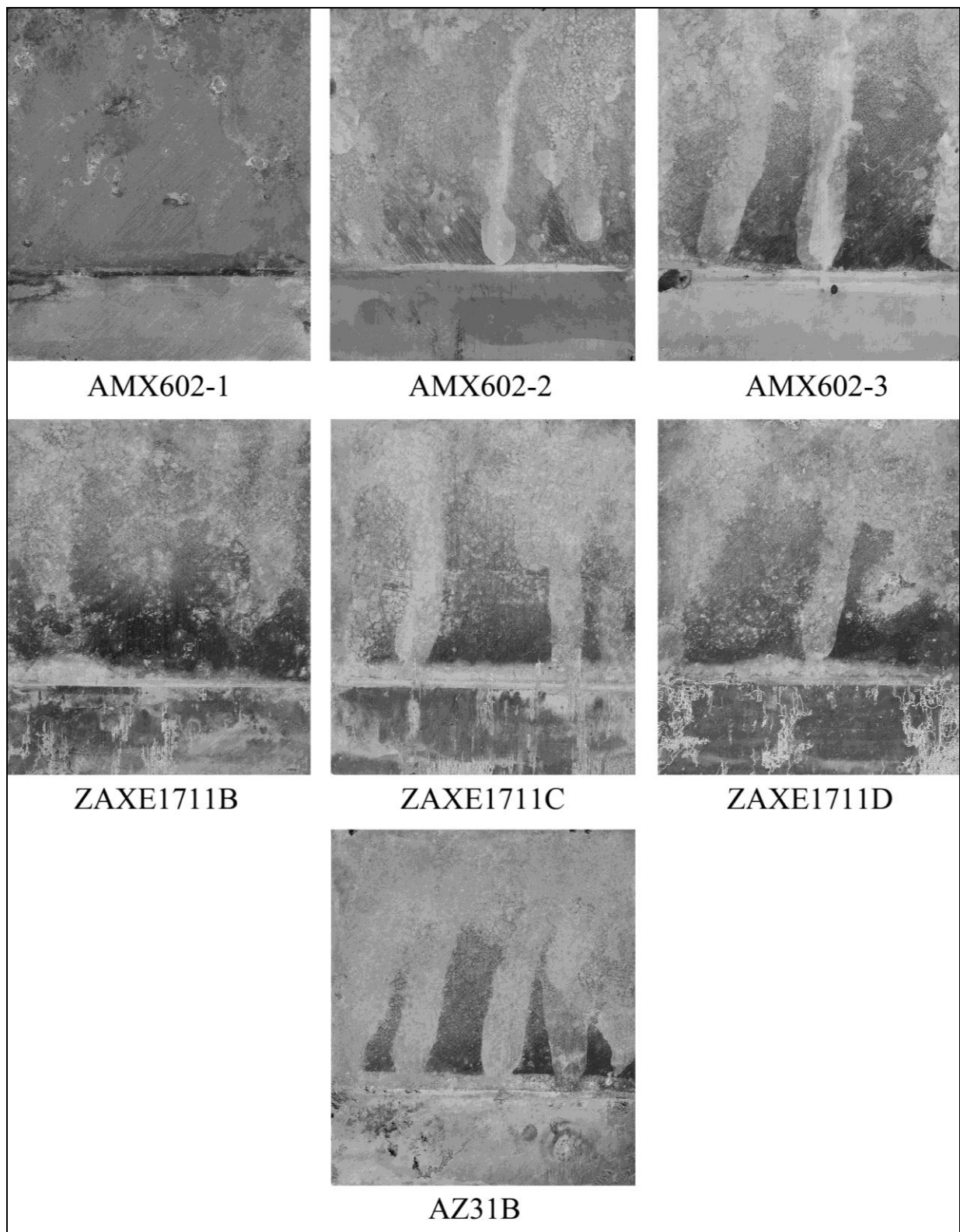


Figure 24. Rear surfaces of 168-h neutral salt fog specimens after cleaning to reveal extent of substrate loss.

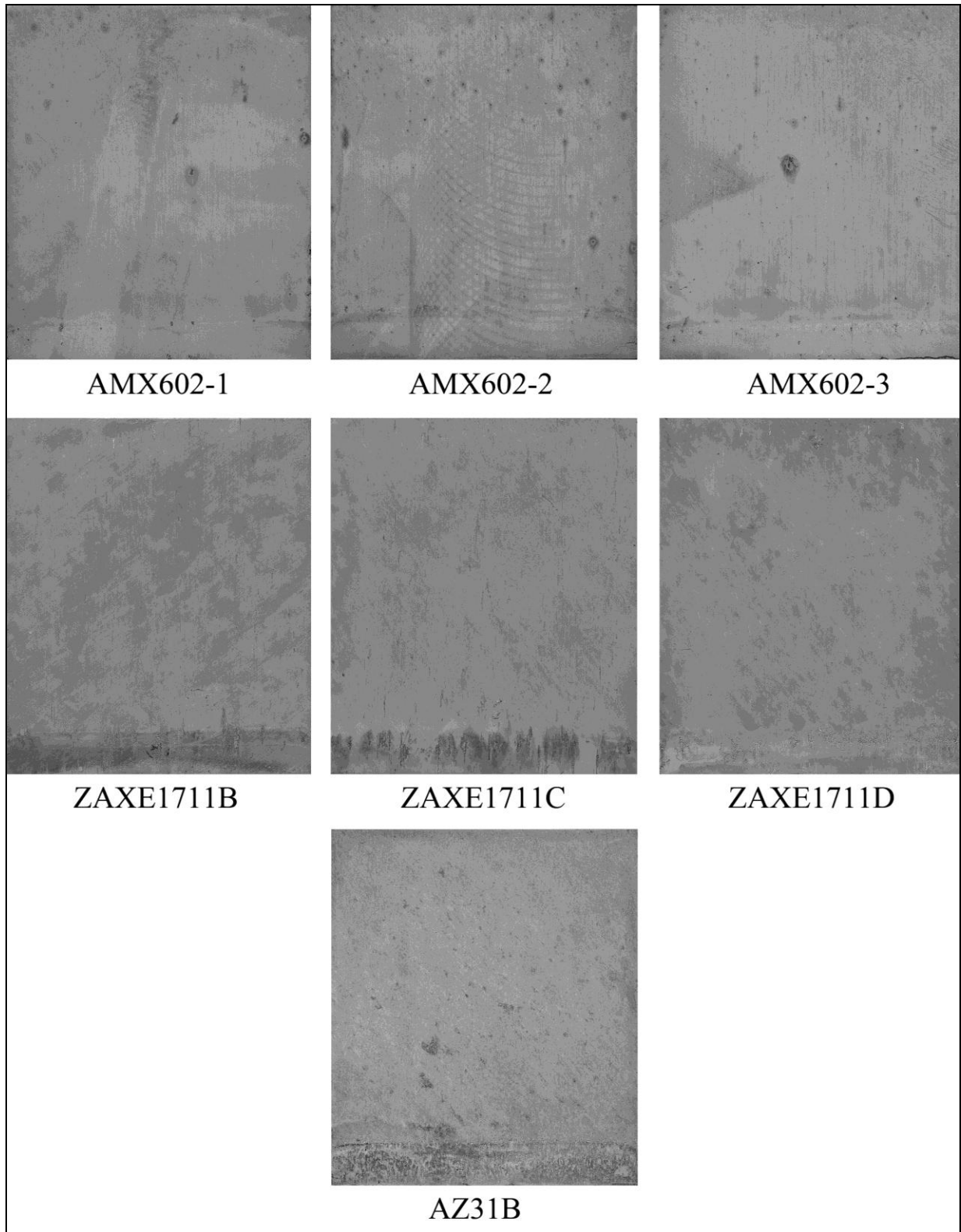


Figure 25. Front surfaces of 10-cycle GM 9540P cyclic corrosion specimens after cleaning to reveal extent of substrate loss.

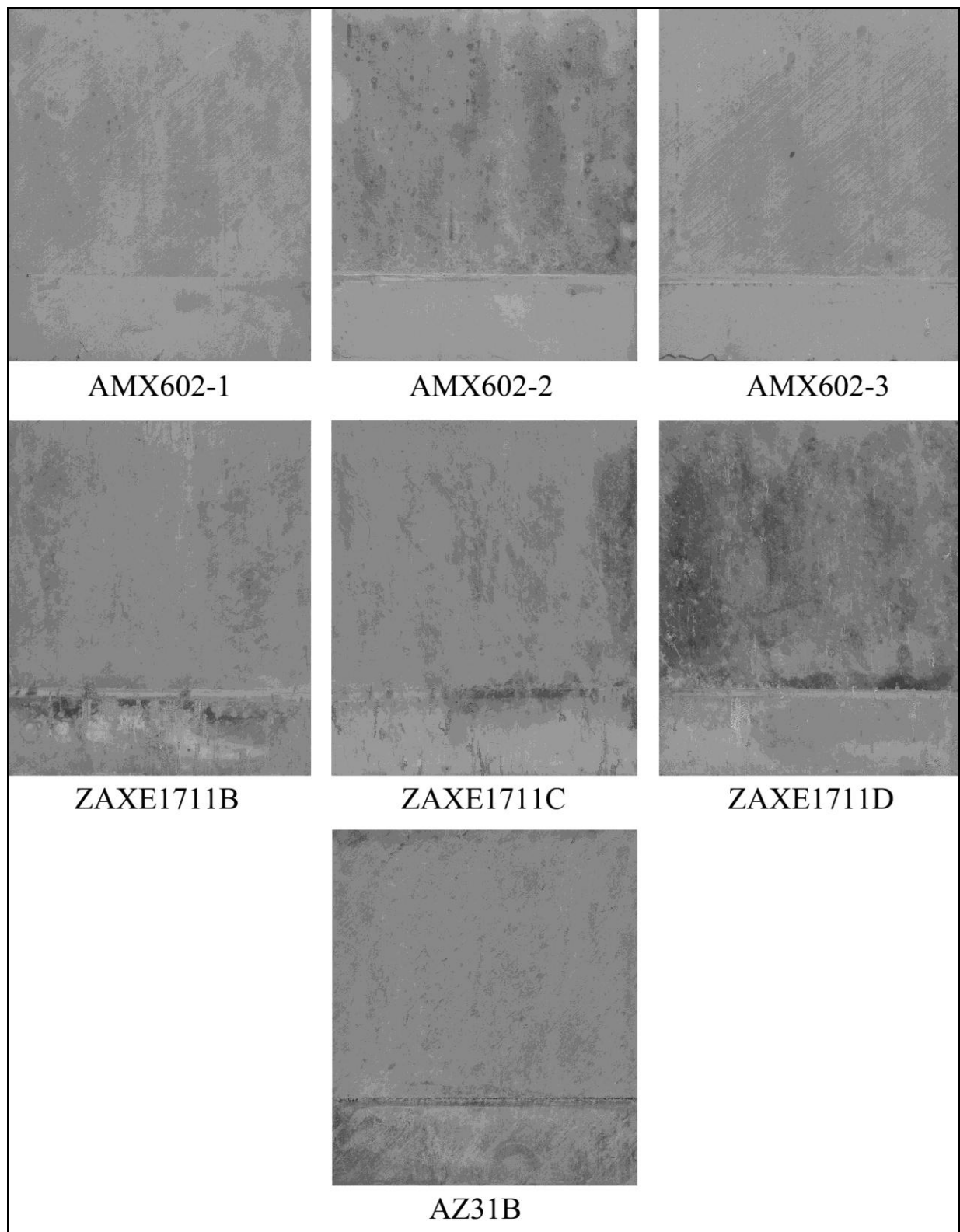


Figure 26. Rear surfaces of 10-cycle GM 9540P cyclic corrosion specimens after cleaning to reveal extent of substrate loss.

3.2.1 AZ31B

As the only Mg alloy that is currently qualified under a MIL SPEC for use as armor plate on U.S. systems, AZ31B-H24 is considered the standard by which all other prospective Mg armor alloys are compared. When initially proposed for armor, the AZ31B-H24 alloy was selected for its combination of good mechanical properties, ballistics, and corrosion resistance. For neutral salt fog, the AZ31B-H24 performed within the mass loss acceptance parameters established for it in the MIL SPEC at 4.7 mpy_{B117}. The neutral salt fog corrosion began as filiform attack and then progressed inward as pits and outward to encompass larger areas by the exposure conclusion at 168 h. The corrosion observed under GM 9540P was less severe than for salt fog. Its progression followed a more general mode and was characterized by dark staining and fine pits.

3.2.2 AMX602

As in AZ31B, AMX602 alloy uses Al as its primary alloying addition. The AMX602 performed well for all three tempers in both neutral salt fog and GM 9540P and finished under the 7.5 mpy_{B117} permissible allowed mils per year limit established for AZ31B. Filiform corrosion attack was more prevalent among the AMX602 specimens than was observed for AZ31B. Similar to AZ31B, the filiform sites progressed to pits during the latter stages of the 1-week exposure. In particular, temper 2 of the AMX602 showed more severe pitting than was observed among any of the other specimens, and the associated corrosion rate determination from mass loss was in agreement. Similar to AZ31B, the GM 9540P, characterized by a dark staining, was much less severe. Interestingly, the GM 9540P exposure revealed prior milling marks in the AMX602-2 specimen, suggesting either over-aggressiveness on the part of the machinist, some degree of sensitivity of the temper to additional heating, or a combination of both. The corrosion rate derived from the mass loss on AMX602-2 under GM 9540P was not the highest among the three AMX602 tempers, suggesting the milling discolorations observed were primarily cosmetic and did not significantly degrade the corrosion resistance. Overall, the degree of observed corrosion under the GM test was even less than observed for AZ31B and was confirmed via the corrosion rates determined from the mass loss data for the associated specimens.

3.2.3 ZAXE1711

Similar to AMX602, the ZAX alloy performed very well under neutral salt fog and GM 9540P cyclic conditions. The ZAXE1711 was also under the 7.5 mpy_{B117} permissible mils per year limit established for AZ31B across all three tempers. As with the AZ31B and the AMX602, the observed corrosion was more severe for neutral salt fog than for GM 9540P, and once again, the corrosion rates from mass loss measurements confirmed the trend. The ZAXE1711 specimens showed the greatest degree of filiform attack and even showed small traces of it under the GM exposure. Once again, there was reasonable agreement between the quantity of observed corrosion and the corrosion rates from mass loss measurements. Similarly, the degree of observed corrosion for the GM procedure was much less than for neutral salt fog and was confirmed via the mass loss measurements.

3.3 Cyclic Polarization Results

Potentiodynamic polarization of metal surfaces can provide information about the ability of a material to resist corrosion. The potential is usually ranged from cathodic to anodic potentials through the OCP for a given alloy. The resulting cathodic and anodic curves can be analyzed, and the Tafel slopes from those curves can be used to give the corrosion potential and the corrosion rate for an alloy in a given environment. When a potentiodynamic approach is used, the corrosion susceptibility of Mg alloys AMX602(1-3), ZAXE1711(B-D), and AZ31B was compared.

The electrochemical behavior of the Mg alloys suggests that corrosion inhibition observed for the new AMX602 and ZAXE1711 series alloys is similar to that of the AZ31B alloy. The polarization curves in figure 27 represent the best of the AMX602 and ZAXE1711 alloys as compared to AZ31B.

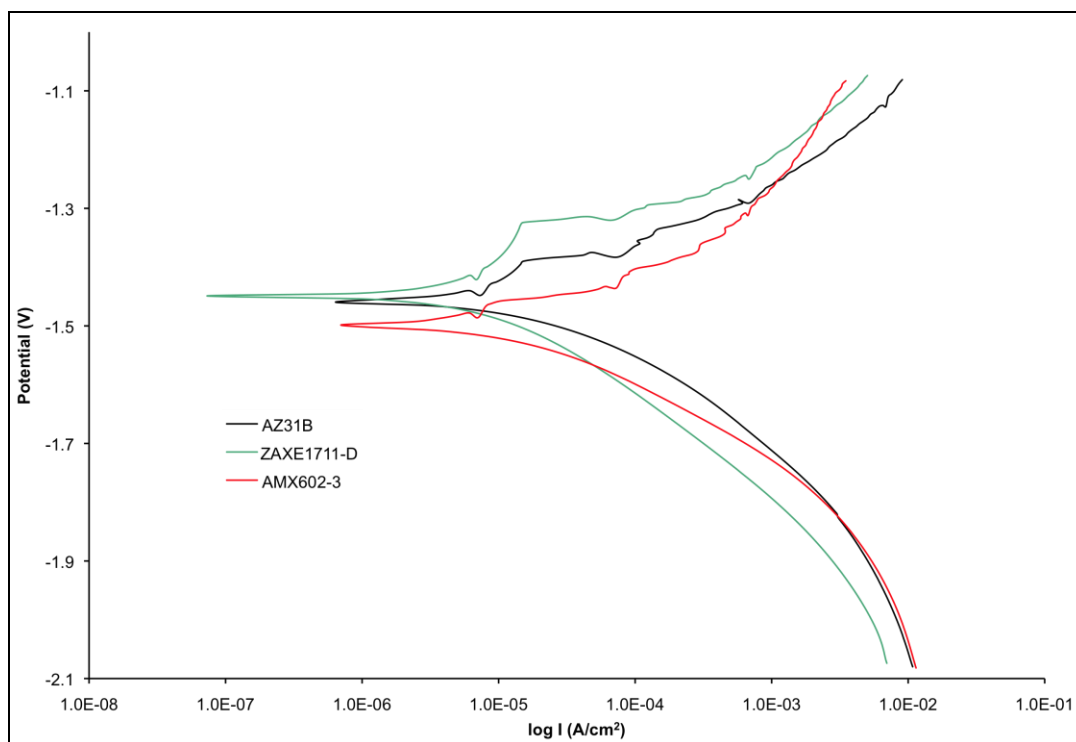


Figure 27. Potentiodynamic polarization of AMX602-3, ZAXE1711-D, and AZ31B alloys.

The OCP of the AMX602 alloys was slightly lower (~30 mV) than that of AZ31B (figure 28), whereas the OCP of the ZAXE1711 alloys was slightly higher (~10–25 mV) than that of AZ31B (figure 29). The current densities measured for all of the alloys as a function of potential were also similar (figures 28 and 29). The minute differences in the polarization behavior of these alloys is consistent with the results of the standard exposure (vide supra) that suggest the corrosion performance of ZAXE1711, and AMX Mg alloys is similar to AZ31B.

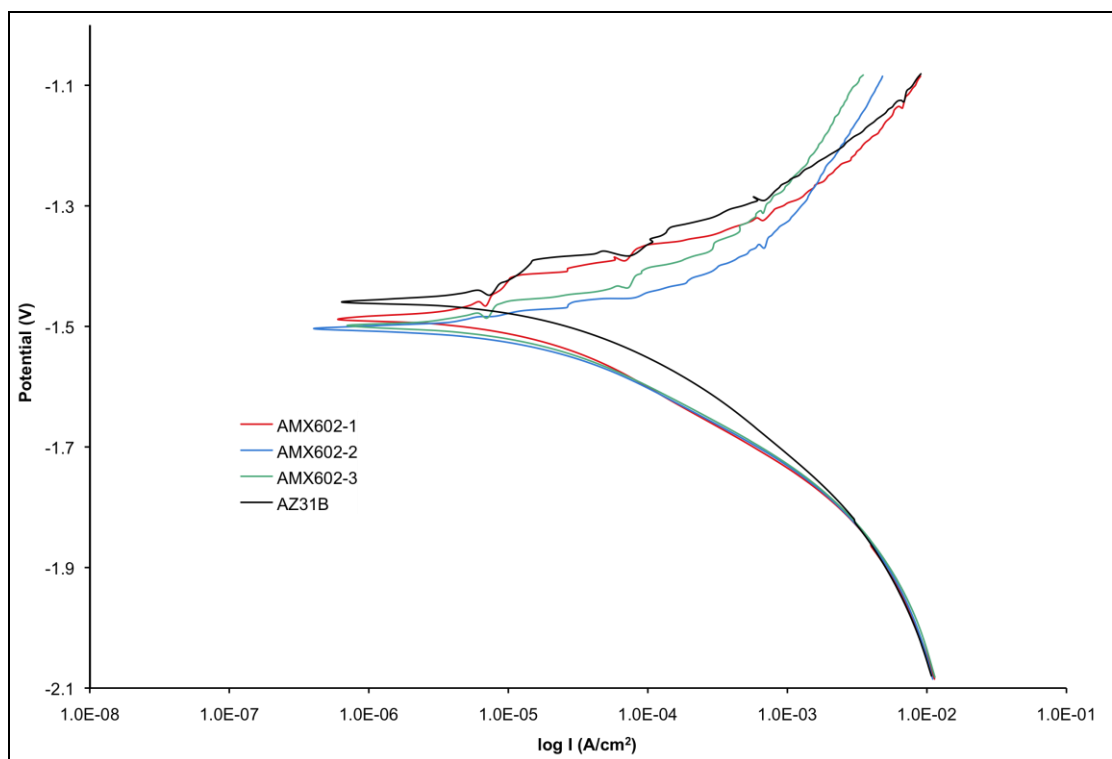


Figure 28. Potentiodynamic polarization of AMX602 and AZ31B alloys.

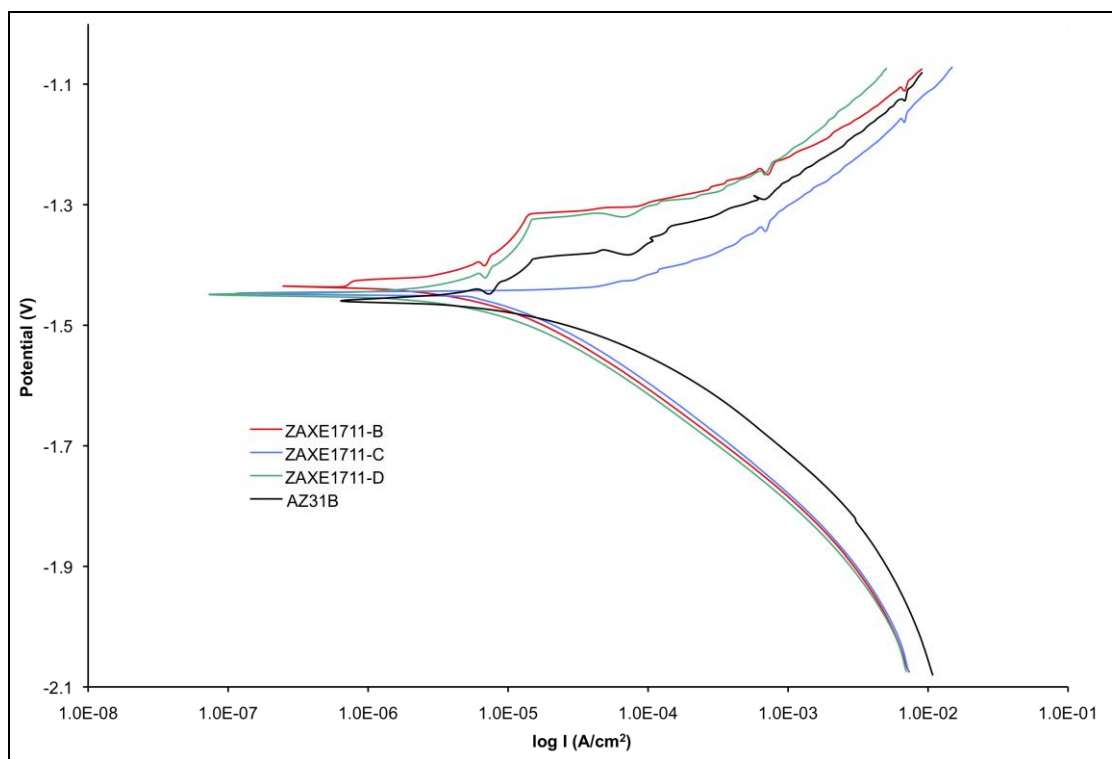


Figure 29. Potentiodynamic polarization of ZAXE1711 and AZ31B alloys.

4. Discussion

The continual drive for increased protection for troops and ground equipment has not only led to penalties in mission performance from increased weight and mobility losses, it has also increased costs from fuel consumption and increased service intervals due to increased mechanical wear and tear from higher structural loading. To counter these consequences, there has been a renewed emphasis on lighter-weight materials, including composites and Mg alloys, that extends beyond their traditional roles in aviation. The inherent environment for ground equipment differs greatly from aviation, and many additional mission factors such as soil, water, vibration, and shock from weapons operation, fastener configurations, and a variety of other design constraints must be considered. The AZ31B Mg alloy that is the basis for MIL-DTL-32333 (5) was an excellent reference point because of its wide use and balance of desirable properties, including strength, ballistics, and corrosion resistance. This balance of properties is key to the use of Mg alloys in the Army. There are many Mg alloys that are stronger than AZ31B and others with better corrosion resistance than AZ31B (18). In order to advance the state of the art for protection based upon Mg plate, any new alloy must possess all of these desirable properties. Based upon their measured mechanical properties, ballistics, and corrosion resistance, the experimental AMX602- and ZAXE1711-series alloys thus far appear to be a very good prospect for further gains in Mg armor performance.

The high ballistic limits and limited spallation on the target impacts for both the AMX602 and the ZAXE1711 were even more impressive when the limited cross sections of the target bars were considered. Additionally, the lack of cracking when impacts were in very close proximity reflects the high degree of ductility inherent to these alloys. It is hypothesized that ballistic limits will further improve when larger plate geometries are introduced for these alloys.

Similar to AZ31B, Al is the primary alloying element in many of the new Mg alloys and generally increases corrosion resistance with increasing concentration. While the curves generated from the potentiodynamic scans were too complex to produce reliable Tafel slopes, the overall shapes and proximities of the curves on the plots, in addition to the accelerated corrosion observations, further indicate similar overall corrosion behavior to AZ31B by the AMX602 and ZAXE1711 alloys. The AZ61 and AZ91 alloys typically exhibit even greater corrosion resistance than AZ31B, mainly because of their increased Al percentages. AZ91E at 9% Al, in particular, is considered among the best for corrosion resistance among all Mg alloys. While the use of Al as an alloying element is the foundation for many corrosion-resistant Mg alloys, it is not the only viable means, nor is it a singular basis, for producing corrosion-resistant alloys. Recent work from Sudholz et al. (19), shown in figure 30, demonstrated in AZ91E that a variety of any single small alloying additions can produce significant changes in corrosion resistance. Their trial using Ca showed a significant drop in current density vs. the AZ91E control. Overall,

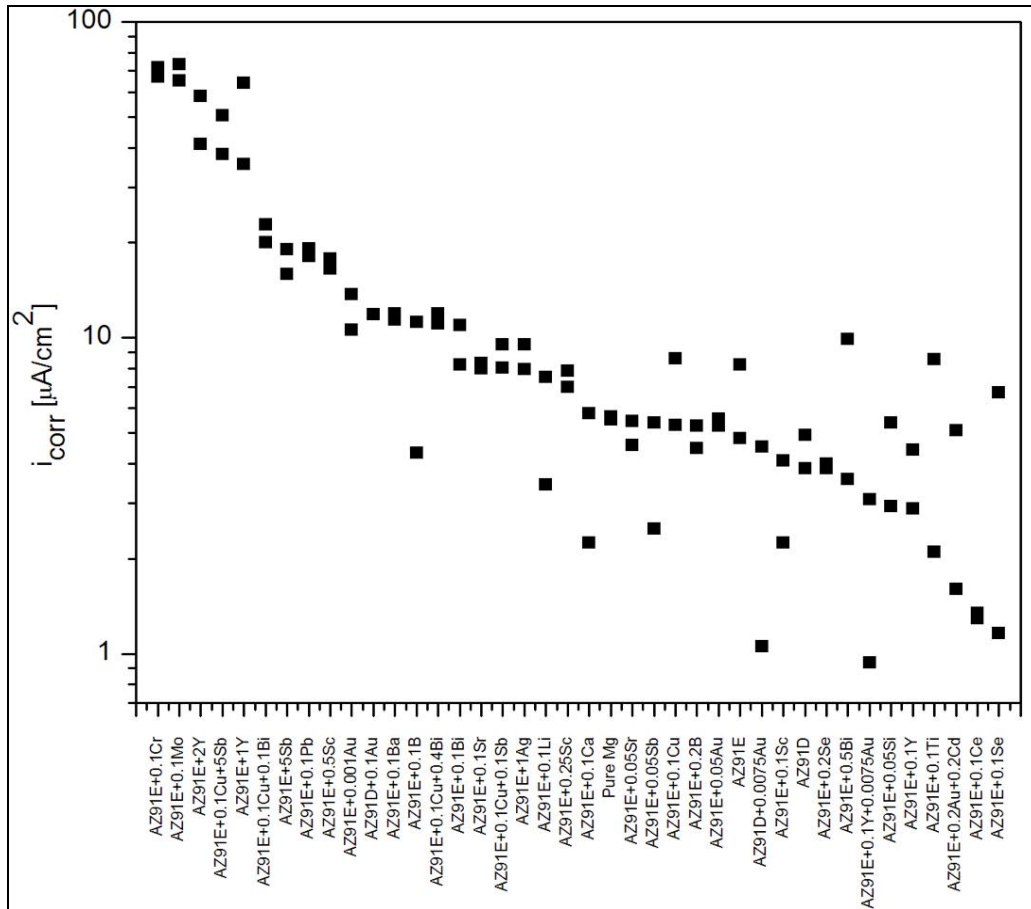


Figure 30. Corrosion rate as a function of composition for Mg alloy AZ91E with a quaternary alloying addition. Testing in 0.1 M NaCl pH 6 (18).

Ca appears to carry much merit for many factors, including corrosion resistance, flame resistance (20), and decreased cost through reduced use of rare earth alloying additions. The use of Ca as an alloying element in the AMX602 and ZAXE1711 alloys may contribute to their good corrosion performance.

For further gains in protection by using Mg alloys, the mechanical properties and ballistic performance must increase while maintaining or even increasing the corrosion resistance found in AZ31B. The AMX602 and ZAXE1711 alloys should be considered successful in this regard, and their continued development would be prudent. Ultimately, and as with every successful Mg alloy application, due diligence in design to include component geometries (e.g., rounded edges), proper drainage to avoid moisture traps, coatings selection, and electrical isolation from other materials under wet conditions are all absolute necessities.

5. Conclusions

The following list describes the findings from the ballistic and corrosion evaluation of these nascent Mg alloys:

- New Mg alloy AMX602 and Mg alloy ZAXE1711 bars showed superior ballistic performance as an armor alloy when compared to baseline Mg armor alloy AZ31B plate.
 - Initial ballistic performance results of Mg alloys AMX602 and ZAXE1711 showed up to 33% and 37% higher ballistic limits, respectively, when compared to the baseline AZ31B Mg armor alloy.
 - Advanced powder metallurgy processing and chemical alloying achieved superior mechanical and corrosion-resistant properties.
 - Corrosion rates measured under neutral salt fog for all tempers of AMX602 and ZAXE1711 were well within the 7.5 mpy acceptance range from the MIL-DTL-32333 (5) Mg armor specification.
 - Corrosion rates (mils per year) were higher under neutral salt fog than under GM 9540P across all alloys and tempers, and visual assessments confirmed the higher aggressiveness of the salt fog environment.
 - Potentiodynamic scans across all tempers of AMX602 and ZAXE1711 revealed only minimal variations in current densities across the range of voltages, thus further confirming similar corrosion resistance to AZ31B.
 - The combination of superior ballistics, high strength, and good corrosion resistance with little or no rare earth alloying additions revealed in this study indicates great potential for these alloys and reveals a likely path for even greater improvements in the future.
-

6. Future Work

Future development will include the scaling up of Mg alloy AMX602 bars to plate for further analysis and full-scale structural applications with similar scaling up efforts planned for ZAXE1711, pending successful results. It is expected that the ballistic limit and thus the overall ballistic performance of the scaled size will increase because of reduced edge effects during an impact.

Additional post scale-up corrosion studies to assess coatings and fastener compatibility are planned.

7. References

1. Jones, T.; DeLorme, R.; Burkins, M.; Gooch, W. *Ballistic Evaluation of Magnesium Alloy AZ31B*; ARL-TR-4077; U.S. Army Research Laboratory: Aberdeen Proving Ground, MD, 2007.
2. Mathaudhu, S.; Nyberg, E. Magnesium Alloys in Army Applications: Past, Current and Future Solutions. *Proceedings From the Minerals, Metals and Materials (TMS) Annual Symposium*, Seattle, WA, 2010.
3. Jones, T.; DeLorme, R. *Development of a Ballistic Specification for Magnesium Alloy AZ31B*; ARL-TR-4664; U.S. Army Research Laboratory: Aberdeen Proving Ground, MD, 2008.
4. Jones, T.; DeLorme, R. A Comparison of the Ballistic Performance Between Rolled Plate in AZ31B-H24 Magnesium and 5083-H131 Aluminum. *Proceedings From the International Symposium on Ballistics*, New Orleans, LA, 2008.
5. MIL-DTL-32333 (MR). *Armor Plate, Magnesium Alloy, AZ31B, Applique* **2009**.
6. Jones, T.; Kondoh, K. *Initial Evaluation of Advanced Powder Metallurgy Magnesium Alloys for Dynamic Applications*; ARL-TR-4828; U.S. Army Research Laboratory: Aberdeen Proving Ground, MD, 2009.
7. Liao, J. M.; Hotta, K.; Kaneko, K.; Kondoh, K. Enhanced Impact Toughness of Magnesium Alloy by Grain Refinement. *Scripta Materialia* **2009**, 61, 208–211.
8. Sakamoto, M.; Akiyama, S.; Hagio, T.; Ogi, K. Control of Oxidation Surface Film and Suppression of Ignition of Molten Mg-Ca Alloy by Ca Addition. *Journal of Japan Foundry Engineering Society* **1997**, 69, 227–233.
9. Nishida, S.; Motomura, I. Estimation of Heat Transfer Coefficient and Temperature Transition on Melt Drag Process of AZ31 Magnesium Alloy by Heat Transfer and Solidification Analysis. *Journal of Japan Institute of Light Metals* **2008**, 58, 439–442.
10. Kondoh, K.; Hamada, E. A.; Imai, H.; Umeda, J.; Jones, T. L. Microstructures and Mechanical Responses of Powder Metallurgy Non-Combustive Magnesium Extruded Alloy by Rapid Solidification Process in Mass Production. *Journal of Materials and Design* **2010**, 31, 1540–1546.

11. Jones, T.; Kondoh, K. The Development of Superior Magnesium Alloy AMX602 Using a Novel Rapid Solidification Process for Structural Applications. *Proceedings From the Materials Science & Technology Conference & Exhibition*, Houston, TX, 2010.
12. MIL-STD-662F. *V₅₀ Ballistic Test for Armor* **1997**.
13. MIL-DTL-46593B. *Projectile, Calibers 0.22, 0.30, 0.50, and 20 MM Fragment-Simulating* **2006**.
14. ASTM B 117-90. Standard Method of Salt Spray (Fog) Testing. *Annu. Book ASTM Stand.* **1990**.
15. GM 9540P. Accelerated Corrosion Test. *General Motors Engineering Standards* **1997**.
16. Miller, C.; Placzankis, B.; Kidd, J.; Luckner, J. *Assessment of Aviation Coating Systems Performance Using Accelerated Test Methods*; ARL-TR-3428; U.S. Army Research Laboratory: Aberdeen Proving Ground, MD, February 2005.
17. ASTM G 97-97. Standard Test Method for Laboratory Evaluation of Magnesium Sacrificial Anode Test Specimens for Underground Applications. *Annu. Book ASTM Stand.* **2007**.
18. Placzankis, B.; Miller, C.; Mathaudhu, S.; Delorme, R. Corrosion Comparisons Among Magnesium Alloys of Interest for DOD Systems Using Laboratory Based Accelerated Corrosion Methods. NACE Paper No. 10085, Corrosion 2010 Conference and Expo., San Antonio, TX, March 2010.
19. Sudholz, A. D.; Birbilis, N.; Bettles, C. J.; Gibson, M. A. Corrosion Behaviour of Mg-Alloy AZ91E With Atypical Alloying Additions; *Journal of Alloys and Compounds* **2009**, 471, 109.
20. Choi, B.; You, B.; Park, W.; Huang, Y.; Park, I. Effect of Ca Addition on the Oxidation Resistance of AZ91 Magnesium Alloys at Elevated Temperatures. *Metals and Materials International* **2003**, 9 (4), 395–398.

INTENTIONALLY LEFT BLANK.

Appendix A. AMX602 Ballistic Data and Pictures

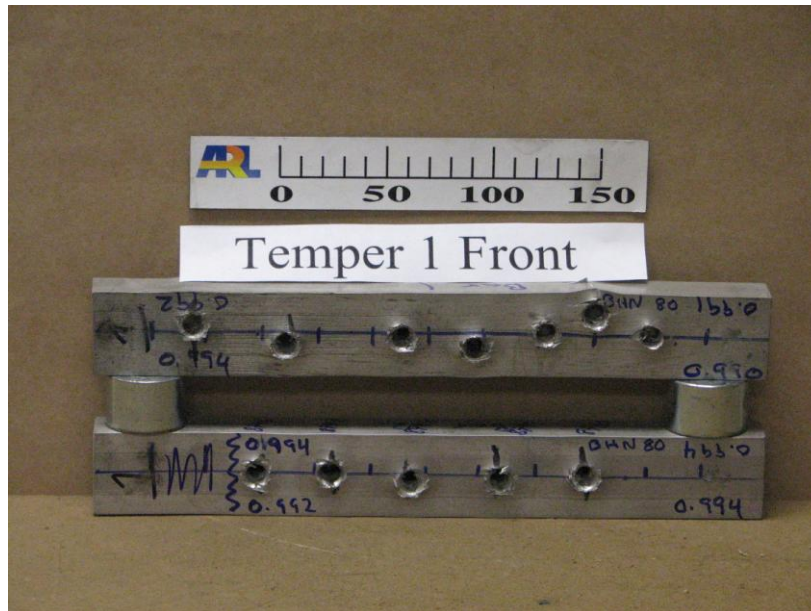
This appendix appears in its original form, without editorial change.

Target:	AMX602-1 Mg Plate				29-Sep-09		
Temper:	300°C				EF106		
Thickness:	Bar 1	25.190	mm	0.992	"		
	Bar 2	25.235	mm	0.994	"		

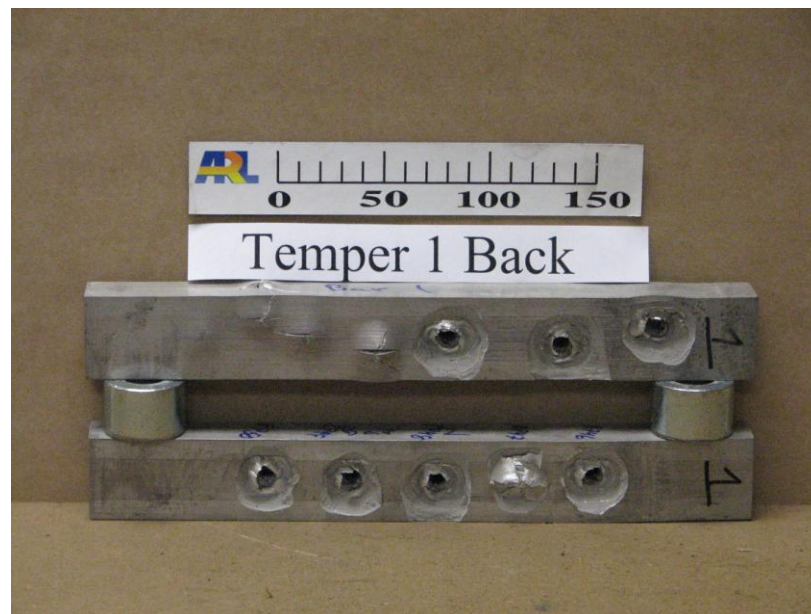
Hardness:	80 BHN on 500kg scale						
Obliquity:	0°						
Projectile:	0.30-cal FSP						
Low CP:	1061	m/s		Low CP:	3482	ft/s	
High PP:	1066	m/s		High PP:	3499	ft/s	
V50:	1061	m/s		V50:	3480	ft/s	
Std Dev:	10	m/s		Std Dev:	34	ft/s	
ZMR:	5	m/s		ZMR:	17	ft/s	
# shots:	6			# shots:	6		
Spread:	27	m/s		Spread:	88	ft/s	
Striking Velocity (m/s)	Striking Velocity (ft/s)	Pitch (deg)	Yaw (deg)	Result (PP/CP)	Used for V50	Comments	Shot #
844	2769	--	--	PP	N	--	8739
932	3059	--	--	PP	N	--	8740
943	3094	--	--	PP	N	--	8741
1022	3354	--	--	PP	N	--	8742
1068	3504	--	--	CP	Y	--	8743
1031	3382	--	--	PP	N	Spall dented witness	8744
1068	3504	--	--	CP	Y	--	8745
1061	3482	--	--	CP	Y	--	8746
1029	3375	--	--	PP	N	Spall dented witness	8747
1066	3499	--	--	PP	Y	Spall dented witness	8748
1041	3416			PP	Y	Spall dented witness	8749
1058	3472			PP	Y	Spall dented witness	8750

Temper 1

Bar 1 and Bar 2, Front



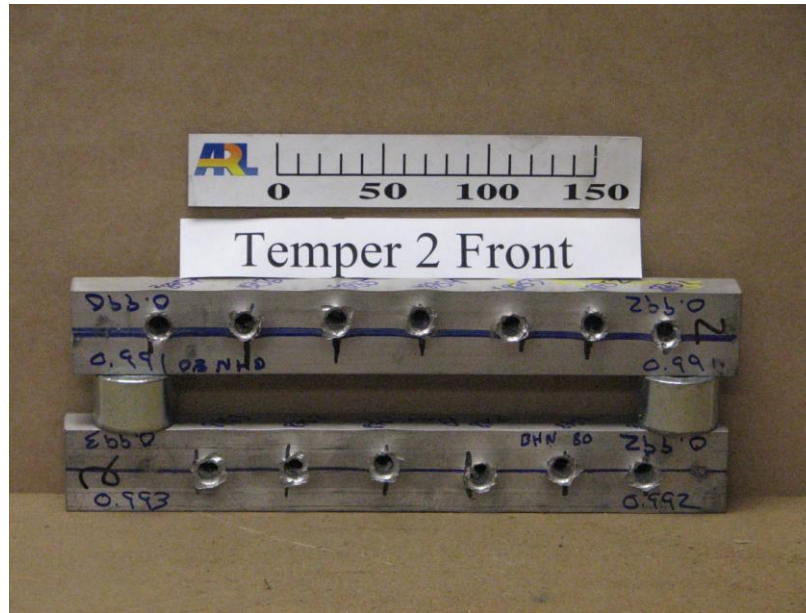
Bar 1 and Bar 2, Back



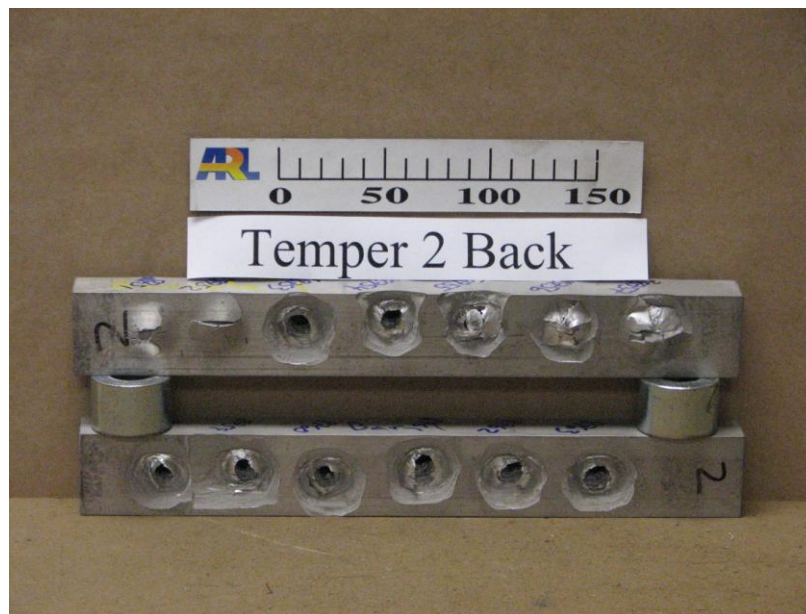
Target:	AMX602-2 Mg Plate				1-Oct-09			
Temper:	350°C				EF106			
Thickness:	Bar 1	25.171	mm	0.991	"			
	Bar 2	25.210	mm	0.993	"			
	Bar 3	25.197	mm	0.992	"			
=====								
Hardness:	80 BHN for Bars 1 & 2; 83 BHN for Bar 3 on 500kg scale							
Obliquity:	0°							
Projectile:	0.30-cal FSP							
Low CP:	1086	m/s		Low CP:	3563	ft/s		
High PP:	1090	m/s		High PP:	3576	ft/s		
V50:	1092	m/s		V50:	3581	ft/s		
Std Dev:	6	m/s		Std Dev:	21	ft/s		
ZMR:	4	m/s		ZMR:	13	ft/s		
# shots:	4			# shots:	4			
Spread:	15	m/s		Spread:	48	ft/s		
Striking	Striking	Pitch	Yaw	Result	Used	Comments	Shot	
Velocity	Velocity				for V50		#	
(m/s)	(ft/s)	(deg)	(deg)	(PP/CP)				
1038	3406	--	--	PP	N	Spall dented w itness	8751	Bar 1
1031	3381	--	--	PP	N	--	8752	"
1086	3563	--	--	CP	Y	--	8753	"
1064	3491	--	--	PP	N	Spall dented w itness	8754	"
1076	3529	--	--	PP	N	Spall dented w itness	8755	"
1068	3504	--	--	PP	N	--	8756	"
1071	3515	--	--	PP	N	--	8757	"
1111	3645	--	--	CP	N	Spall dented w itness	8758	Bar 2
1090	3575	--	--	PP	Y	--	8759	"
1126	3694	--	--	CP	N	--	8760	"
1101	3611	--	--	CP	Y	Spall dented witness	8761	"
1076	3531	--	--	PP	N	--	8762	"
1117	3663	--	--	CP	N	--	8763	"
1090	3576	--	--	PP	Y	Spall dented witness	9282	Bar 3

Temper 2

Bar 1 and Bar 2, Front



Bar 1 and Bar 2, Back



Temper 2

Bar 3, Front



Bar 3, Back

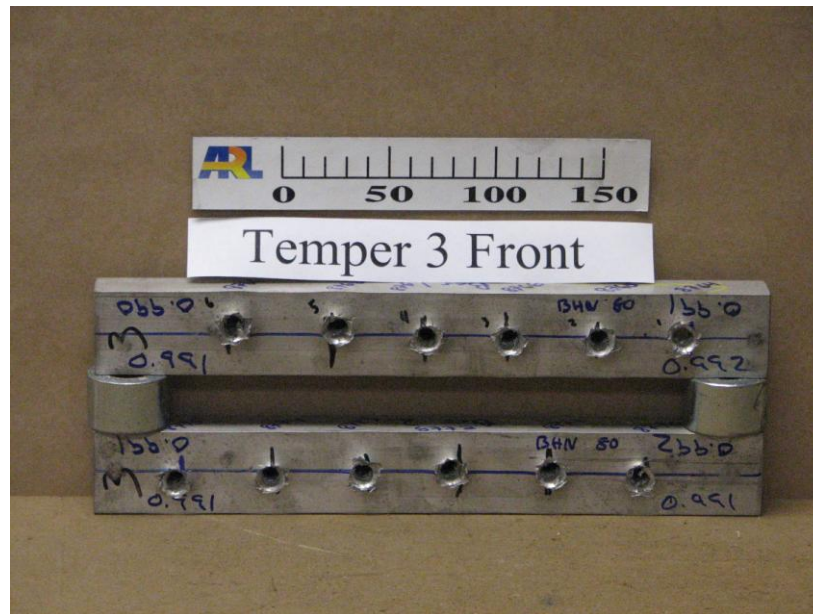


Target:	AMX602-3 Mg Plate				5-Oct-09		
Temper:	250°C				EF106		
Thickness:	Bar 1	25.171	mm	0.991	"		
	Bar 2	25.178	mm	0.991	"		

Hardness:	80 BHN on 500kg scale						
Obliquity:	0°						
Projectile:	0.30-cal FSP						
Low CP:	1090	m/s		Low CP:	3577	ft/s	
High PP:	1131	m/s		High PP:	3709	ft/s	
V50:	1105	m/s		V50:	3624	ft/s	
Std Dev:	19	m/s		Std Dev:	63	ft/s	
ZMR:	40	m/s		ZMR:	132	ft/s	
# shots:	10			# shots:	10		
Spread:	56	m/s		Spread:	185	ft/s	
Striking Velocity (m/s)	Striking Velocity (ft/s)	Pitch (deg)	Yaw (deg)	Result (PP/CP)	Used for V50	Comments	Shot #
1086	3563	--	--	PP	Y	Spall dented witness	8764
1131	3709	--	--	PP	Y	Spall dented witness	8765
1093	3586	--	--	CP	Y	--	8766
1092	3583	--	--	PP	Y	Spall dented witness	8767
1151	3776	--	--	CP	N	--	8768
1142	3748	--	--	CP	Y	--	8769
1090	3577	--	--	CP	Y	--	8770
1091	3578	--	--	CP	Y	--	8771
1077	3534	--	--	PP	N	Spall dented witness	8772
1106	3630	--	--	PP	Y	Spall dented witness	8773
1097	3600	--	--	PP	Y	Spall dented witness	8774
1117	3664	--	--	CP	Y	--	8775

Temper 3

Bar 1 and Bar 2, Front



Bar 1 and Bar 2, Back



Appendix B. ZAXE1711 Ballistic Data and Pictures

This appendix appears in its original form, without editorial change.

Target:	ZAXE1711				29-Mar-10			
Temper:	B				EF106			
Thickness:	Bar 1	25.248	mm	0.994	"			
Hardness:	80 BHN on 500kg scale							
Obliquity:	0°							
Projectile:	0.30-cal FSP							
Low CP:	1114	m/s		Low CP:	3654	ft/s		
High PP:	1105	m/s		High PP:	3626	ft/s		
V50:	1111	m/s		V50:	3646	ft/s		
Std Dev:	8	m/s		Std Dev:	27	ft/s		
ZMR:	0	m/s		ZMR:	0	ft/s		
# shots:	4			# shots:	4			
Spread:	18	m/s		Spread:	58	ft/s		
Striking Velocity	Striking Velocity	Pitch	Yaw	Result	Used	Comments	Shot	
(m/s)	(ft/s)	(deg)	(deg)	(PP/CP)	for V50		#	
1135	3723	--	--	CP	N	--	9293	Bar 1
1114	3654	--	--	CP	Y	--	9294	"
1122	3681	--	--	CP	Y	--	9295	"
1104	3623	--	--	PP	Y	--	9296	"
1105	3626	--	--	PP	Y	--	9297	"

Temper B

Bar 1, Entry



Bar 1, Exit



Temper C

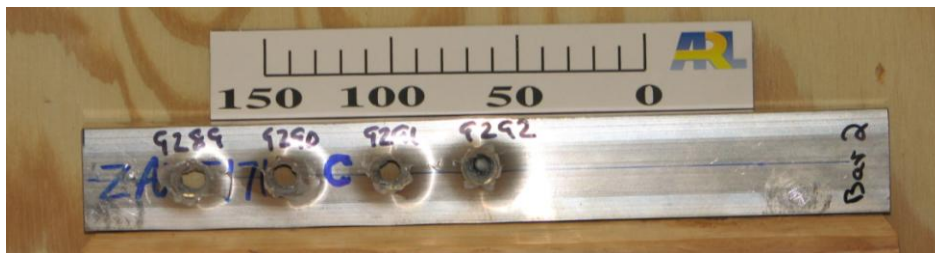
Bar 1, Entry



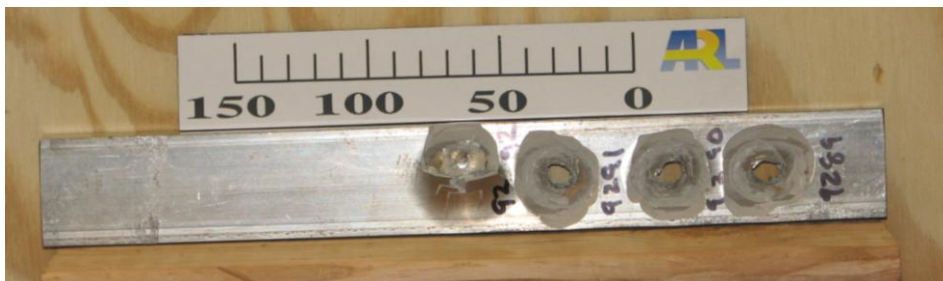
Bar 1, Exit



Bar 2, Entry



Bar 2, Exit



Target:	ZAXE1711				30-Mar-10			
Temper:	D				EF106			
Thickness:	Bar 1	25.210	mm	0.993	"			
	Bar 3	25.279	mm	0.995	"			
Bar 2 not used								

Hardness:	80 BHN on 500kg scale							
Obliquity:	0°							
Projectile:	0.30-cal FSP							
Low CP:	1129	m/s		Low CP:	3702	ft/s		
High PP:	1144	m/s		High PP:	3753	ft/s		
V50:	1140	m/s		V50:	3737	ft/s		
Std Dev:	10	m/s		Std Dev:	33	ft/s		
ZMR:	15	m/s		ZMR:	51	ft/s		
# shots:	6			# shots:	6			
Spread:	24	m/s		Spread:	24	ft/s		
Striking	Striking	Pitch	Yaw	Result	Used	Comments	Shot	
Velocity	Velocity				for V50		#	
(m/s)	(ft/s)	(deg)	(deg)	(PP/CP)				
1117	3662	--	--	PP	N	--	9298	Bar 1
1128	3699	--	--	PP	Y	--	9299	"
1129	3702	--	--	CP	Y	--	9300	"
1144	3753	--	--	PP	Y	--	9301	"
1167	3829	--	--	CP	N	--	9302	"
1106	3628	--	--	PP	N	--	9303	"
1170	3837	--	--	CP	N	--	9304	Bar 3
1152	3778	--	--	CP	Y	--	9305	"
1148	3764	--	--	CP	Y	--	9306	"
1136	3726	--	--	PP	Y	--	9307	"

Temper D

Bar 1, Entry



Bar 1, Exit



Bar 2, Entry



Bar 2, Exit



NO. OF
COPIES ORGANIZATION

1 (PDF only)	DEFENSE TECHNICAL INFORMATION CTR DTIC OCA 8725 JOHN J KINGMAN RD STE 0944 FORT BELVOIR VA 22060-6218
1	DIRECTOR US ARMY RESEARCH LAB IMNE ALC HRR 2800 POWDER MILL RD ADELPHI MD 20783-1197
1	DIRECTOR US ARMY RESEARCH LAB RDRL CIO LL 2800 POWDER MILL RD ADELPHI MD 20783-1197
1	DIRECTOR US ARMY RESEARCH LAB RDRL CIO LT 2800 POWDER MILL RD ADELPHI MD 20783-1197
1	DIRECTOR US ARMY RESEARCH LAB RDRL D 2800 POWDER MILL RD ADELPHI MD 20783-1197

NO. OF
COPIES ORGANIZATION

2 CDR US ARMY TACOM
AMSTA TR S
L FRANKS
D TEMPLETON
MS 263
WARREN MI 48397-5000

1 PM HBCT
SFAE GCS HBCT S
MS 506 J ROWE
6501 E 11 MILE RD
WARREN MI 48397-5000

1 CRUSADER OPM
SFAE GCSS CR E
B ROOPCHAND
BLDG 171A
PICATINNY ARSENAL NJ 07806-5000

3 DARPA
DEFENSE SCIENCE OFC
L CHRISTODOULOU
J GOLDWASSER
S WAX
3701 N FAIRFAX DR
ARLINGTON VA 22203-1714

1 PM BFVS
SFAE GCSS W BV S
M KING
WARREN MI 48397-5000

1 NVL SURFC WARFARE CTR
CARDEROCK DIV
R PETERSON CODE 28
9500 MACARTHUR BLVD
WEST BETHESDA MD 20817-5700

2 LAWRENCE LIVERMORE NATL LAB
R LANDINGHAM L372
J REAUGH L282
PO BOX 808
LIVERMORE CA 94550

2 LOS ALAMOS NATL LAB
F ADDESSIO
M BURKETT
PO BOX 1663
LOS ALAMOS NM 87545

NO. OF
COPIES ORGANIZATION

3 SANDIA NATL LAB
J ASAY MS 1811
L CHHABILDAS MS 1811
D CRAWFORD MS 0836 9116
PO BOX 5800
ALBUQUERQUE NM 87185-0307

1 AIR FORCE ARMAMENT LAB
AFATL DLJW
W COOK
EGLIN AFB FL 32542

4 UNIV OF TEXAS
INST FOR ADVNCD TECH
S BLESS
H FAIR
J HODGE
R SUBRAMANIAN
3925 W BRAKER LN
AUSTIN TX 78759-5316

2 SOUTHWEST RSCH INST
C ANDERSON
J WALKER
6220 CULEBRA RD
SAN ANTONIO TX 78238

2 UNIV OF CA SAN DIEGO
DEPT OF APPL MECH & ENGR
SVC RO11
S NEMAT NASSER
M MEYERS
LA JOLLA CA 92093-0411

1 BRIGGS COMPANY
J BACKOFEN
4192 HALES FORD RD
MONETA VA 24121-5458

3 BAE ADVNCD CERAMICS SYS
R PALICKA
G NELSON
B CHEN
1960 WATSON WAY
VISTA CA 92083

3 GDLS
W BURKE MZ436 21 24
G CAMPBELL MZ436 30 44
D DEBUSSCHER MZ436 20 29
38500 MOUND RD
STERLING HTS MI 48310-3200

NO. OF
COPIES ORGANIZATION

1	RJ R JONES 80 PALISADE AVE WHITE PLAINS NY 10607
3	GDLS J ERIDON MZ436 21 24 W HERMAN MZ435 01 24 S PENTESCU MZ436 21 24 38500 MOUND RD STERLING HTS MI 48310-3200
1	RENSSELAER POLYTECHNIC INST S A JACKSON 110 8TH ST TR 3RD FL TROY NY 12180-3590
1	PENN STATE UNIV APPLIED RSRCH LAB ACOUSTICS PRGM D SWANSON 504L APPLIED SCI BLDG UNIVERSITY PK PA 16803
1	PACIFIC NORTHWEST NATL LAB E NYBERG MSIN P7-82 902 BATTELLE BLVD RICHLAND WA 99352
5	UNIV OF VIRGINIA DEPT OF MTRLS SCI & ENG SCHOOL OF ENG & APPL SCI H WADLEY B214 THORNTON HALL 116 ENGINEERS WAY CHARLOTTESVILLE VA 22903
5	CELLULAR MTRLS INTRNTL INC Y MURTY 1200 FIVE SPRINGS RD STE 201 CHARLOTTESVILLE VA 22903
1	FORCE PROTECTION INDUST INC V JOYNT 9801 HWY 78 LADSON SC 29456
2	US ARMY RSRCH DEV & ENGRG CTR AMSRD NSC IPD B P CUNNIFF J WARD KANSAS ST NATICK MA 01760-5019

NO. OF
COPIES ORGANIZATION

1	THE AIR FORCE RSRCH LAB AFRL/MLLMP T TURNER BLDG 655 RM 115 2230 TENTH ST WRIGHT-PATTERSON AFB OH 45433-7817
1	MISSOURI UNIV OF SCI & TECHLGY R MISHRA B37 MCNUTT HALL ROLLA MO 65409-0340
3	NATL GROUND INTLLGNC CTR D EPPERLY T SHAVER T WATERBURY 2055 BOULDERS RD CHARLOTTESVILLE VA 22911-8318
3	PROG EXECUTIVE OFC – SOLDIER US ARMY DIR TECH MGMT PROJ MGR - SOLDIER EQUIP K MASTERS C PERRITT J ZHENG 15395 JOHN MARSHALL HWY HAYMARKET VA 20169
1	CERADYNE INC M NORMANDIA 3169 RED HILL AVE COSTA MESA CA 92626
1	R3 TECHNOLOGY J RIEGEL 7324 FOUNTAIN SPRING CT SPRINGFIELD VA 22150-4905
2	SOUTHWEST RSRCH INST T HOLMQUIST G JOHNSON 5353 WAYZATA BLVD STE 607 MINNEAPOLIS MN 55416
1	US ARMY RAPID EQUIPPING FORCE R TURNER 10236 BURBECK RD BLDG 361T FORT BELVOIR VA 22060-5806

NO. OF
COPIES ORGANIZATION

2 LETTERKENNY ARMY DEPOT
PRODUCTION ENGRNG DIV
AMSAM LE MO E S
K HERSHEY
J FRIDAY
1 OVERCASH AVE
CHAMBERSBURG PA 17201-4150

1 DIR US ARMY RSRCH LAB
RDRL D
J MILLER
B SMITH
V WEISS
2800 POWDER MILL RD
ADELPHI MD 20783-1197

1 DIR US ARMY RSRCH LAB
RDRL SES A
N SROUR
2800 POWDER MILL RD
ADELPHI MD 20783-1197

1 DIR US ARMY RSRCH LAB
RDRL SES
J EICKE
2800 POWDER MILL RD
ADELPHI MD 20783-1197

1 DIR US ARMY RSRCH LAB
RDRL SF
T BOWER
2800 POWDER MILL RD
ADELPHI MD 20783-1197

1 DIR US ARMY RSRCH LAB
RDRL SE
J PELLEGRINO
2800 POWDER MILL RD
ADELPHI MD 20783-1197

1 DIR US ARMY RSRCH LAB
RDRL SES P
2800 POWDER MILL RD
ADELPHI MD 20783-1197

1 DIR US ARMY RSRCH LAB
RDRL SM
2800 POWDER MILL RD
ADELPHI MD 20783-1197

NO. OF
COPIES ORGANIZATION

5 DIR US ARMY RSRCH OFC
S MATHAUDHU
PO BOX 12211
RESEARCH TRIANGLE PARK
NC 27709-2211

2 TABER EXTRUSIONS LLC
B WETMORE
D MOORE
915 S ELMIRA
RUSSELLVILLE AR 72801

1 OFC NVL RSRCH
D SHIFLER
875 N RANDOLPH ST
CODE 332 RM 631
ARLINGTON VA 22203-1995

1 US ARMY RDECOM
AMSRD NSC IP MC
M CODEGA
1 KANSAS ST
NATICK MA 01760-5000

ABERDEEN PROVING GROUND

1 DIR USA EBCC
SCBRD RT
5183 BLACKHAWK RD
APG EA MD 21010-5424

1 CDR USA SBCCOM
AMSCB CII
5183 BLACKHAWK RD
APG EA MD 21010-5424

1 DIR USAMSAA
AMSRD AMS D
BLDG 392

1 CDR USATEC
STEAC LI LV
E SANDERSON
BLDG 400

1 CDR US ARMY EVAL CTR
TEAE SVB
M SIMON
4120 SUSQUEHANNA AVE
APG MD 21005-3013

NO. OF
COPIES ORGANIZATION

93 DIR USARL
RDRL SL
R COATES
RDRL SLB
R BOWEN
RDRL SLB D
D LOWRY
RDRL SLB W
W BRUCHEY
L ROACH
RDRL VT
S WILKERSON
RDRL WM
L BURTON
B FORCH
S KARNA
J MCCAULEY
P PLOSTINS
W WINNER
RDRL WML
T VONG
M ZOLTOSKI
RDRL WML D
A HORST
RDRL WML E
R ANDERSON
RDRL WML H
T FARRAND
L MAGNESS
D SCHEFFLER
S SCHRAML
R SUMMERS
RDRL WMM
J BEATTY
R DOWDING
RDRL WMM B
B CHEESEMAN
RDRL WMM C
B PLACZANKIS (10 CPS)
J LABUKAS (5 CPS)
RDRL WMM D
R CARTER
E CHIN
K CHO
W ROY
R SQUILLACIOTI
S WALSH
RDRL WMM E
J P SINGH
RDRL WMM F
J CHINELLA
K DOHERTY
V HAMMOND
L KECSKES

NO. OF
COPIES ORGANIZATION

H MAUPIN
D SNOHA
RDRL WMS
T ROSENBERGER
RDRL WMP
P BAKER
B BURNS
S SCHOENFELD
RDRL WMP A
C HUMMER
B RINGERS
RDRL WMP B
C HOPPEL
Y HUANG
M SCHEIDLER
RDRL WMP C
S BILYK
T BJERKE
D CASEM
J CLAYTON
D DANDEKAR
M GREENFIELD
B LEAVY
M RAFTENBERG
S SEGLETES
RDRL WMP D
R DONEY
T HAVEL
R MUDD
J RUNYEON
B SCOTT
W WALTERS
M ZELLNER
RDRL WMP E
M BURKINS
W GOOCH
M KORNECKI
B LOVE
D HACKBARTH
E HORWATH
T JONES (3 CPS)
C KRAUTHAUSER
D LITTLE
D SHOWALTER
P SWOBODA
RDRL WMP F
N GNIAZDOWSKI
R GUPTA
J MONTGOMERY

NO. OF
COPIES ORGANIZATION

- | | |
|---|--|
| 1 | OSAKA UNIVERSITY
JOINING & WELDING RSCH INST
K KONDOH
11-1 MIHOGAOAKA IBARAKI
OSAKA 567-0047 JAPAN |
| 1 | DEFENSE RESEARCH AGENCY
B JAMES
PORTON DOWN
SALISBURY WTTTS SP04 OJQ
UNITED KINGDOM |
| 1 | KATO PROFESSIONAL ENGR OFC
Y KATO
18-22 HIGASHI-TERAO TUSRUMI
YOKOHAMA 230-0018 JAPAN |

INTENTIONALLY LEFT BLANK.